Atmos. Chem. Phys. Discuss., 14, 9275–9343, 2014
www.atmos-chem-phys-discuss.net/14/9275/2014/
doi:10.5194/acpd-14-9275-2014

Atmospheric Chemistry and Physics Discussions

Measurements of the aerosol chemical composition and mixing state in the Po Valley using multiple spectroscopic techniques

S. Decesari[1], J. Allan[2], C. Plass-Duelmer[3], B. J. Williams[4,5], M. Paglione[1], M. C. Facchini[1], C. O'Dowd[6], R. M. Harrison[7,9], J. K. Gietl[7,3], H. Coe[2], L. Giulianelli[1], G. P. Gobbi[1], C. Lanconelli[1], C. Carbone[1], D. Worsnop[4], A. T. Lambe[4], A. T. Ahern[4,], F. Moretti[8], E. Tagliavini[8], T. Elste[3], S. Gilde[3], Y. Zhang[5], and M. Dall'Osto[6,*]**

[1]Institute of Atmospheric Sciences and Climate of the National Research Council of Italy (ISAC-CNR), Bologna, Italy
[2]School of Earth, Atmospheric and Environmental Science, University of Manchester, Manchester, UK
[3]Deutscher Wetterdienst (DWD), Meteorological Observatory, Hohenpeissenberg, Germany
[4]Aerodyne Research, Inc., Billerica, MA, USA
[5]Energy, Environmental & Chemical Engineering, Washington University in St. Louis, St. Louis, USA

[6]School of Physics, National University of Ireland, Galway, Ireland
[7]School of Geography, Earth & Environmental Sciences, University of Birmingham, Birmingham, UK
[8]Centro Interdipartimentale di Ricerca per le Scienze Ambientali, University of Bologna, Bologna, Italy
[9]Department of Environmental Sciences/Center of Excellence in Environmental Studies, King Abdulaziz University, P.O. Box 80203, Jeddah, 21589, Saudi Arabia
[*]now at: Institut de Ciències del Mar, CSIC, Barcelona, Spain
[**]now at: Center for Atmospheric Particle Studies, Carnegie Mellon University, Pittsburgh, PA, USA

Received: 6 March 2014 – Accepted: 18 March 2014 – Published: 4 April 2014

Correspondence to: S. Decesari (s.decesari@isac.cnr.it)

Published by Copernicus Publications on behalf of the European Geosciences Union.

ACPD
14, 9275–9343, 2014

Abstract

The use of co-located multiple spectroscopic techniques can provide detailed information on the atmospheric processes regulating aerosol chemical composition and mixing state. So far, field campaigns heavily equipped with aerosol mass spectrometers have been carried out mainly in large conurbations and in areas directly affected by their outflow, whereas lesser efforts have been dedicated to continental areas characterized by a less dense urbanization. We present here the results obtained in San Pietro Capofiume, which is located in a sparsely inhabited sector of the Po Valley, Italy. The experiment was carried out in summer 2009 in the framework of the EUCAARI project ("European Integrated Project on Aerosol, Cloud Climate Aerosol Interaction"). For the first time in Europe, six state-of-the-art techniques were used in parallel: (1) on-line TSI aerosol time-of-flight mass spectrometer (ATOFMS), (2) on-line Aerodyne high-resolution time-of-flight aerosol mass spectrometer (HR-TOF-AMS), (3) soot particle aerosol mass spectrometer (SP-AMS), (4) on-line high resolution time-of-flight mass spectrometer-thermal desorption aerosol gas chromatograph (HR-ToFMS-TAG), (5) off-line twelve-hour resolution proton nuclear magnetic resonance (H-NMR) spectroscopy, and (6) chemical ionization mass spectrometry (CIMS) for the analysis of gas-phase precursors of secondary aerosol.

Data from each aerosol spectroscopic method were analysed individually following ad-hoc tools (i.e. PMF for AMS, Art-2a for ATOFMS). The results obtained from each techniques are herein presented and compared. This allows us to clearly link the modifications in aerosol chemical composition to transitions in air mass origin and meteorological regimes. Under stagnant conditions, atmospheric stratification at night and early morning hours led to the accumulation of aerosols produced by anthropogenic sources distributed over the Po Valley plain. Such aerosols include primary components such as black carbon (BC), only partly internally mixed with secondary semivolatile compounds such as ammonium nitrate and amines. Other organic components originating from anthropogenic sources at night include monocarboxylic acids which correspond

ACPD
14, 9275–9343, 2014

to an AMS factor analogous to the "cooking" organic aerosol (COA) already identified in urban areas. In daytime, enhanced mixing in the planetary boundary layer (PBL) along with increasing temperature determined dramatic changes in aerosol composition caused by the evaporation of semivolatile components and by the entrainment of aged aerosols transported downwards from residual layers. In other words, the entrainment of aged air masses is responsible for the accumulation of low-volatility oxygenated organic aerosol (LV-OOAs) and also for the recycling of primary species such as black carbon. The LV-OOA concentrations were shown to correlate to the simple meteorological tracers of humid PBL air produced by daytime convection over land areas. In particular, both PMF-AMS and PMF-NMR could resolve two components of LV-OOA: one from long-range transport from Central Europe, the second from recirculated PBL air from the Po Valley. According to organic aerosol source apportionment by PMF-AMS, anthropogenic aerosols accumulating in the lower layers overnight accounted for 38 % of organic aerosol mass on average, another 21 % was accounted for by aerosols recirculated in residual layers but still originating in North Italy, while a substantial fraction (41 %) was due to the most aged aerosols imported from transalpine areas.

Overall, the deployment of six state-of-the-art spectrometric techniques provided a comprehensive picture of the nature and source contributions of aerosols and aerosol precursors at a European rural site with unprecedented level of details.

1 Introduction

Mass Spectrometry of Atmospheric Aerosol (MSAA) has recently been established and has quickly become the most essential and fastest growing area of aerosol research (Laskin et al., 2012). Such techniques have greatly enhanced our capacity of observing the atmospheric processes responsible for the formation and evolution of airborne particles. However, currently none of the MSSA instruments is ideal in terms of both recovery and identification level because the individual techniques differ in terms of sensitivity towards specific aerosol components. Hence, the use of co-located complementary

ACPD
14, 9275–9343, 2014

spectroscopic methods has becoming a prerequisite for large field experiments dealing with ambient aerosol chemical characterization. In the recent years, several of such experiments took place within or in the proximity of megacities and other large metropolitan areas: MILAGRO in Mexico City (Doran et al., 2007), SOAR and CalNex in Los Angeles (Docherty et al., 2008; Hayes et al., 2013), REPARTEE in London (Harrison et al., 2012), MEGAPOLI in Paris (Healy et al., 2013), SAPUSS in Barcelona (Dall'Osto et al., 2013). Alternatively, supersites were located in rural areas but still with the aim of characterize the export of pollutants from very large conurbations, such as the New York area (NEAQS–ITCT, Fehsenfeld et al., 2006). Less attention has been paid to land sites where urbanization is less dense and urban, agricultural and (semi)natural lands are intermingled in complex mosaics, which is a common situation for many continental areas. In Europe, for instance, the total number of inhabitants of the five megacities (Istanbul, Moscow, London, Paris, Rhine-Ruhr) account for only 11 % of the total urban population in the continent (ca. 550 millions, source: UNEP). The experimental strategy of intercepting pollution plumes and linking aerosol characteristics to transport time, which proved to be successful in metropolitan areas and in downwind areas, cannot work for aerosol studies at supersites surrounded by complex patterns in land use and emission types. We present here the results obtained in the Po Valley in summer 2009 during an intensive field campaign organized in the frame of the EUCAARI project (Kulmala et al., 2011). The Po Valley counts 20 millions of inhabitants but spread over an area of 48 000 km^2. Urbanization is more dense in the northern sector of the valley and extended areas of mainly agricultural land are found in the central and south-east sectors. The station where the field campaign took place, San Pietro Capofiume (SPC) is located in the middle of such "periphery" of the Po Valley, in a sparsely populated, flat rural area in the southeast part of the valley. It is recognized that the Po Valley is a major European pollution hotspot due to a high intensity of anthropogenic sources and to the orography which can limit atmospheric dispersion of pollutants. Nevertheless, the actual impacts of specific sources and of atmospheric dynamics is expected to vary considerably during the year in an area characterized by hot and dry summers and

ACPD
14, 9275–9343, 2014

moderately cold winters. In previous papers (Saarikoski et al., 2012; Paglione et al., 2013), we showed that aerosol concentration and chemical composition in rural Po Valley during late winter and early spring are governed by a reduced vertical mixing in the low troposphere, accumulating combustion particles and secondary aerosols in the low altitude levels. Contrasting dynamics are found in the summer, when the atmosphere is very convective with mixing layer height normally reaching 1500–2000 m above the ground (Di Giuseppe et al., 2012), making the Apennine ridge in the south border of the valley a permeable barrier for extended transport. To the north of the Po Valley, Henne et al. (2004) have shown that aerosol-rich boundary layer air lifted by thermally-driven valley breezes can cross the Alp mountain system. This means that in principle the Po Valley cannot be considered a "closed system" during the summer season. In previous studies in the area, observations of aerosol chemical composition were carried out with traditional samplers coupled with off-line analysis (Carbone et al., 2010). A major limitation of the off-line analyses is that, due to the poor time resolution (12–24 h), they can observe variations in aerosol chemical composition over timescales which are much longer than those typical of the meteorology. Here, we employ modern spectroscopic aerosol instrumentation to investigate for the first time aerosol concentration and composition at a background site during the summertime in the Po Valley (from 28 June to 12 July 2009) at high time resolution (1 h). We investigate secondary organic aerosol production, nitrate production, and source apportionment of organic aerosol. The experiment can be considered representative for other heavily populated areas characterized by a dry summer, intense photochemistry, and by complex orography, which is a common situation in subtropical areas of Eurasia and North America.

ACPD
14, 9275–9343, 2014

2 Methodology

2.1 Measurement site

San Pietro Capofiume (SPC, 44°23′ N, 11°22′ E, 11 m a.s.l.) is a site placed in an agricultural area between the cities of Bologna and Ferrara (roughly 40 km from both cities). According to the EMEP criteria, SPC is a rural background site (distance from major pollution sources: 10–50 km, Larssen et al., 1999). The station hosts meteorological measurements run by the environmental protection agency (ARPA) of region Emilia-Romagna. In addition, observations of fog chemistry, fog-aerosol interaction, aerosol optical properties analysis and aerosol chemical characterization studies have been coordinated by CNR since the late 80s. The first aerosol mass spectrometric measurements were performed at SPC during a first EUCAARI field campaign in March–April 2008 (Saarikoski et al., 2012).

2.2 Meteorological measurements and atmospheric profiling

Temperature, relative humidity, wind intensity and direction and precipitation were measured in continuous mode at 6 m above the ground using a WXT510 (Vaisala) station. Atmospheric aerosol vertical profiling was provided by a commercial LiDAR-Ceilometer, Vaisala LD-40 working with a 855 nm laser. In addition to aerosol loads, signal analysis allowed to track the BL evolution by using aerosols as markers. Planetary boundary layer measurements obtained during the campaign are discussed in the paper by Di Giuseppe et al. (2012).

2.3 Gas-phase composition

Concentrations of ozone were furnished by the Emilia-Romagna monitoring network for atmospheric pollution. CIMS (chemical ionization mass spectrometry) provided direct measurements of sulphuric acid concentrations in the gas-phase. It also quantified OH radical concentration, which in turn was used to estimate production rates of sul-

ACPD
14, 9275–9343, 2014

phuric acid and nitric acid starting from the measured concentrations of sulphur dioxide and NO_2. Gaseous sulphuric acid and OH-radicals were measured by DWD-CIMS as previously described by Berresheim et al. (2000), Rohrer and Berresheim (2006), and Plass-Duelmer et al. (2011). The instrument was set up in a container and sampled air from a height of 3 m above ground, 0.5 m above the container. Basically, OH is chemically titrated by addition of SO_2 to yield H_2SO_4, H_2SO_4 is then selectively ionized by NO_3^- ions at atmospheric pressure, and the resulting ions are transferred into a vacuum chamber. Here, water clusters are broken up and the HSO_4^- ions are analysed by mass spectrometry. The system has a sensitivity of 2×10^5 molecules cm^{-3} and an estimated accuracy of 30 %. In addition to sulphuric acid, also malonic acid (MA) and methanesulphonic acid (MSA) are ionized by nitrate ions and detected at their corresponding masses by MS in the DWD CIMS. Though several attempts were undertaken to directly calibrate these compounds from vaporized mixtures, no reliable direct calibration was achieved. Consequently, we used as a rough estimate the same calibration factor for MA and MSA as for H_2SO_4 in this paper. Furthermore, during the campaign SO_2 was measured by a fluorescence sensor (Thermo, TE 43 S), NO by chemiluminescence with O_3 (ECO-Physics CLD 770AL ppt), and NO_2 by photolytic conversion (ECO-Physics) and measurement as NO (Gilge et al., 2010). Finally, photolysis frequencies of NO_2 and ozone to yield $J(O^1D)$ were measured by sets of up- and downward looking filter radiometers (MetCon).

2.4 Off-line aerosol chemical determinations.

The size distribution of main aerosol chemical compounds was measured using 5-stage Berner impactors and off-line chemical analysis (Matta et al., 2003). Daytime and night-time samples were collected separately every 12 h with substrates changed at 9:00 and 21:00 LT (8:00 and 20:00 UTC+1). The substrates were extracted with deionized water and analysed by ion chromatography, total organic carbon (TOC) analysis and NMR spectroscopy.

ACPD
14, 9275–9343, 2014

Anions were separated and quantified on a Dionex ICS-2000 ion chromatograph, equipped with an IonPac AS11 2 × 250 mm Dionex separation column. Cations were analysed with the same ion chromatograph, equipped with an IonPac CS16 3 × 250 mm Dionex separation column for the analysis of both inorganic species (sodium, ammonium, potassium, magnesium, calcium) and organic bases (methyl-, dimethyl-, trimethyl-, ethyl- and diethyl-ammonium). Water-soluble organic carbon (WSOC) was determined using a nitrogen and carbon analyser Analytik Jena Multi N/C 2100S (Rinaldi et al., 2007). The instrument operated in TOC modality, and WSOC was calculated as the difference between total soluble carbon and inorganic carbonate, directly measured by the analyser.

Functional group characterization was performed by proton-Nuclear Magnetic Resonance (^{1}H-NMR) spectroscopy. PM_1 samples were collected separately for daytime and night-time conditions (changing the filters at 9 a.m. and 9 p.m., local time). Spectra of aerosol WSOC were recorded at 600 MHz with a Varian Inova 600 spectrometer. From 400 to 800 scans were acquired for each spectrum depending on the concentration. The HOD peak was suppressed by presaturation using a PRESAT pulse sequence. A 1 Hz line broadening (LB) weighting function and baseline correction was generally applied. After processing the spectra, a 0.03 ppm binning on the chemical shift was applied to generate the matrix of data for factor analysis. The integrals of the spectra was set to the total NMR concentrations as $\mu mol\,H\,m^{-3}$ for the specific samples. Finally, bins containing peaks from blanks were removed. The resulting matrix dimension was 28 samples × 186 points (NMR chemical shift bins). Factor analysis for spectral deconvolution was performed using a sub-set of the algorithms introduced in a previous publication (Decesari et al., 2011). Specifically: EPAv3.0 PMF ("Positive Matrix Factorization," Paatero and Tapper, 1994), NMF ("Non-Negative Matrix Factorization") employing a projected gradient bound-constrained optimization (Lin, 2007), and MCR ("Multivariate Curve Resolution") using the alternating least square method (MCR-ALS, Tauler, 1995; Jaumot et al., 2005). The uncertainty of the measurements for PMF was calculated as three times the baseline noise on the binned spectra. The

ACPD
14, 9275–9343, 2014

selection of the number of factor was essentially based on the comparability of the solutions from the three algorithms, as other diagnostics (Q/Q_{exp}, Paatero and Tapper, 1994) did not provide clear transitions in the explained variations with increasing factor number (Fig. S1).

2.5 On-line aerosol mass spectrometric measurements

A variety of in-situ spectrometric techniques were applied to determine the chemical composition of fine particulate matter in the Po Valley during the summer of 2009. Reported here are experimental set-ups of the following instruments: aerosol time-of-flight mass spectrometer (ATOFMS), high-resolution time-of-flight aerosol mass spectrometer (HR-ToF-AMS), soot particle aerosol mass spectrometer (SP-AMS), and a HR-ToF mass spectrometer thermal desorption aerosol gas chromatograph (HR-ToFMS-TAG).

1. The *ATOFMS* collects bipolar mass spectra of individual aerosol particles. Ambient aerosol is focused into a narrow particle beam for sizes between 100 nm and 3 µm. Using a 2-laser velocimeter, particle sizes are determined from particle velocity after acceleration into the vacuum. In addition, the light scattered by the particles is used to trigger a pulsed high power desorption and ionization laser (λ = 266 nm, about 1 mJ pulse^{-1}) which evaporates and ionizes the particle in the centre of the ion source of a bipolar reflectron ToF-MS. Thus, a positive and negative ion spectrum of a single particle are obtained (Gard et al., 1997).

2. The Aerodyne High-Resolution Time-of-Flight Aerosol Mass Spectrometer (*HR-ToF-AMS*) (DeCarlo et al., 2006; Canagaratna et al., 2007) focuses aerosol particles in the size range 50–600 nm onto a hot surface (~ 600 °C) using an aerodynamic lens assembly (Jayne et al., 2000). Smaller and larger particles (up to 1000 nm) are also collected with lower efficiency. Non-refractory particle components flash-evaporate on the hot surface; the evolving vapour is electron ionized (70 eV) and the ions are transported into an orthogonal extraction ToF-MS for high-resolution mass analysis. Particle size information is obtained by mod-

ACPD
14, 9275–9343, 2014

ulating the particle beam and collecting mass spectra as a function of particle flight time. The instrument provides 5 min averages of mass concentrations of the non-refractory aerosol components as well as species-resolved size distributions (Drewnick et al., 2005). The instrument provides quantitative mass loading information on non refractory components using a well characterised series of calibrations and error estimations (Jimenez et al., 2003; Allan et al., 2003b, 2004). The HR-ToF-AMS (DeCarlo et al., 2006) was deployed in the standard configuration, taking both mass spectrum (MS) and particle time of flight (pToF) data. The MS mode was run in "V-mode" with a mass resolution of up to 3000 $m/\Delta m$ alternatively with a "W-mode", which increases resolution to 6000 $m/\Delta m$ but decreases sensitivity by approximately one order of magnitude. The instruments were calibrated using 350 nm monodisperse ammonium nitrate particles and based on previous experience in urban environments, a collection efficiency (CE) of 0.5 was assumed, in line with the parameterized treatments of Middlebrook et al. (2012).

3. The *SP-AMS* makes real-time, in situ measurements of black carbon containing particles (Onasch et al., 2012). By using an active Nd:YAG (1064 nm) laser cavity in place of the tungsten vaporiser, the SP-AMS uses laser-induced incandescence of absorbing soot particles to vaporize both the coatings and elemental carbon cores within the ionization region of the AMS, providing a unique and selective method for measuring the mass of the refractory carbon cores (i.e., black carbon mass), the mass and chemical composition of any coating material (e.g., organics, sulphates, nitrates, etc.), and particle size and morphology. The data presented here are absolutely quantitative because at the time of the experiment, a calibration protocol had not been developed, however the temporal trends should still be accurate.

4. The *HR-ToFMS-TAG* system provides hourly speciated organic aerosol composition. Fine particles are inertially impacted into a collection and thermal desorption (CTD) cell, then desorbed into a gas chromatograph for chemical separation and

ACPD
14, 9275–9343, 2014

finally delivered to an electron impact HR-ToFMS for compound identification and quantification. The TAG measurement technique (Williams et al., 2006) and interface to an HR-ToFMS has been described previously (Williams et al., 2014)

2.6 Black carbon measurements

A single wavelength particle soot absorption photometer (PSAP) manufactured by Radiance Research was used to measure the aerosol volume absorption coefficient σ_a at 573 nm, through a filter based technique (Bond et al., 1999; Virkkula et al., 2005). BC mass concentrations were calculated assuming a mass absorption cross section (MAC) of 10 $m^2 g^{-1}$ (Zanatta et al., 2014). The exact MAC, as well as its variability during the campaign are unknown. On the other hand, the very good correlation between the BC mass concentrations derived by light absorption (PSAP) with those directly measured by the SP-AMS indicates that MAC did not vary significantly during the experiment (see the discussion below).

3 Results

3.1 Air mass classification and planetary boundary layer (PBL) meteorology

July 2009 was wetter and colder than typical July conditions with respect to the climatology. No heat waves were observed during the measurement campaign. The experiment is therefore more representative for background conditions in the Po Valley in the summer, and does not include high temperature anomalies.

HYSPLIT back-trajectories were classified into six clusters, with two of them reflecting a longer range transport from Western Europe and the Atlantic ("West"), and the other 4 clusters reflecting a weaker circulation with more pronounced local (Po Valley) component ("PoV") (see Fig. S2).

The PoV clusters can be divided into N, ENE, WNW and S/SW categories according to average direction of arrival to SPC. According to these criteria for air mass classi-

ACPD
14, 9275–9343, 2014

fications (see Table S1), the conditions encountered during the Po Valley, 2009 field study can be summarised in three parts: (1) PoV type air masses prevailed during the first week of campaign, and were followed by (2) an outbreak of westerly (Atlantic) air masses on 8–9 July, and finally by (3) a partial recovery of more stable conditions characterized the last two days, with an increasing easterly component in the circulation ("PoV ENE").

The boundary layer meteorology was investigated using a lidar ceilometer aiming to capture major transitions in atmospheric stratification between 100 and 5000 m above the ground caused by sharp gradients in aerosol extinction (Di Giuseppe et al., 2012). With the exception of precipitation days, the "classical" development of a turbulent mixing layer in the morning following the dissipation of a stable nocturnal surface layer can be observed. The transition usually occurred at 9–10 a.m. local time. A striking feature of the ceilometer profiles during the first week of measurement was the intensification of light extinction from aerosol-rich residual layers (Fig. S3), providing evidence for entrainment processes sustaining aerosol concentrations at the ground after turbulent mixing diluted the pre-existing "nocturnal" particles. The progressive aerosol accumulation in residual layers between 500 and 2000 m above the ground on the first days of July are a consequence of the establishment of more stable high pressure conditions and of the cease of afternoon deep convection over the mountains surrounding the valley in the last days of June when it caused some ventilation of the PBL. The existence of residual layers associated with the transport of pollutants up to 3000 m a.s.l. over the Po Valley was first recorded by Crosier et al. (2007).

3.2 Ozone and NO_x chemistry

Our observations of ozone and nitrogen oxides are in line with previous studies in the area. Deserti et al. (2010) have shown that during the sunny summer days, when air is stagnant and ozone pollution extends over a wide area in the Po Valley basin, ozone is transported aloft in atmospheric layers at various altitudes, with a maximum around the top of the PBL (ca. 2000 m a.s.l.). In the morning, ozone is entrained from the resid-

ACPD
14, 9275–9343, 2014

ual layers into the mixing layer leading to an increase of concentrations recorded at ground level which superimposes upon the photochemical source term. At night, when a surface layer is re-established, ozone is removed by dry deposition and titration by NO_x, and concentrations drop. At the same time, NO_x accumulates at night due to reduced atmospheric dispersion and reduced chemical sinks (Fig. S4). Such anticorrelation between the NO_x and O_3 diurnal cycles is triggered by changes in atmospheric stratification and typical for continental rural sites, especially over plains and lowlands, and where the VOC concentrations are simply too small to account for the morning increase in ozone concentrations (Kleinman et al., 1994). The greater focus of this study is not ozone formation but aerosol production, and significant concentrations of secondary aerosol precursors were indeed recorded in San Pietro Capofiume during the experiment, as explained in the following section.

3.3 Gas-phase secondary inorganic and organic species from CIMS

The impact of in-situ photochemistry on the formation of inorganic secondary aerosols from nitrogen and sulphur dioxides was investigated by chemical ionization mass spectrometry (CIMS). The OH radical concentrations reached 1.0×10^7 cm^{-3} around midday and were approximately constant during the experiment. SO_2 concentrations were small, always below the instrument detection limit during night-time, and reaching 1.0 ppb or 1.5 ppb in days characterized by continental air masses ("PoV" types from W, N or E sectors) (Fig. S4). The SO_2 concentrations observed during periods of PoV SW or West air mass types were very small. Daily cumulative production rates of sulphuric and nitric acid from SO_2, NO_2 and OH measurements were calculated from 10 min integrated production rates (Fig. 1, middle panel). There is additionally another source of H_2SO_4 from reactions of Criegee radicals with SO_2, but this term was estimated to contribute some 20 % to the H_2SO_4 budget (Plass-Dülmer et al., 2011), and is in line with low VOC concentrations. The cumulative formation of nitric acid on a daily basis varied between 10 and 30 µg m^{-3}, showing that local HNO_3 production is much higher than what is incorporated into the aerosol typically in the second half of the night, when

ACPD
14, 9275–9343, 2014

temperatures are lowest and relative humidity exceeds 80 % (see the AMS data in the following sections). Thus, NO_2 oxidation by OH can account for the observed local production of aerosol nitrate. With respect to sulphuric acid, the gas phase is depleted rapidly and all H_2SO_4 condenses and is detected as sulphate aerosol (deposition to the ground should be a smaller loss path). The daily cumulative H_2SO_4 production rates of 0.1–0.6 $\mu g\,m^{-3}$ are roughly in line with diurnal variations in the aerosol sulphate (additionally there is oxidation in the aerosol of SO_2) (again see next section for HR-ToF-AMS). However, sulphate is also transported to the site, and is likely also exported from the site. Thus, even if aerosol sulphate and HNO_3 + aerosol nitrate are advected to SPC through the PBL dynamics highlighted above, local production also takes place.

With respect to speciated gas-phase organic compounds measured with the CIMS, malonic acid (MA) and methansulphonic acid (MSA) were detected during the campaign. Malonic acid in particular can be a candidate (or at least a proxy) for semivolatile gas phase oxygenated organics. It is interesting to note that malonic acid has a diurnal cycle very closely related to temperature (maximum in the afternoon) and is completely lost at night (Fig. 1, lower panel), pointing to a source from evaporation from aerosols and/or surfaces which is superimposed upon the photochemical source. Reported concentrations for malonic acid are uncalibrated, but reach ca. 10 ppt around midday assuming a calibration factor equal to that of sulphuric acid. On the other hand, MSA concentrations are below detection limit during daytime and reach daily maxima in the evening when [OH] goes down to nocturnal levels. Such diurnal patterns are inconsistent with the typical breeze regime at the site (from the coast in afternoon hours, and seaward at night), therefore the observed behaviour cannot be fully explained by a marine source for MSA.

3.4 Size-segregated aerosol composition from multistage impactors

We discuss here the outcomes of chemical analyses (ion chromatography and TOC) of multistage impactor samples collected over 12 h time periods. The results are used to

ACPD
14, 9275–9343, 2014

introduce the main features of size-distributions and day-by-day variability of the main refractory and non-refractory aerosol chemical components. Figure 2 reports composition averaged over the subperiods identified in Sect. 3.1 on the basis of meteorological conditions and back-trajectories.

Days from 28 June to 4 July were characterized by relatively high concentrations, especially at night, due to large accumulation mode aerosols (~ 0.4–1 µm) rich in ammonium, nitrate, sulphate and water-soluble organic compounds. A constant night-time composition throughout the first week of the experiment indicates a persistent source of secondary inorganic species and of carbonaceous particles from ground-level sources in the Po Valley, because these samples were collected in conditions of atmospheric stratification. The daytime concentrations were significantly lower than at night on the first days (28–29 June), while in the following days the daytime concentrations converged towards night-time levels. The progressive, day-by-day build-up of aerosol daytime concentrations was concomitant to the accumulation of aerosols in residual layers (Fig. S3). The convergence of the daytime chemical composition towards the nocturnal (nitrate-rich) composition can be explained by supposing that the particles re-circulated from the entrainment of residual layers actually originated from ground-level sources in the Po Valley. In other words, particles from Po Valley sources accumulated every night in a shallow stable surface layer and were ventilated every morning during the mixing layer formation, and, after several days in stagnant conditions, this process caused the entire PBL to fill with such particles, so that the mixing layer formation did not cause significant dilution anymore.

On 5 July, after a strong precipitation event during the previous night, concentrations were small for all species, with the exception of sulphate and water-soluble organics. The period of westerly air masses (7 to 9 July) showed greater concentrations of coarse particles with respect to previous days, with a lot of seasalt and nitrate (Fig. 3). The size-distribution of nitrate is completely skewed in fine size range. The presence of coarse mode sea salt in "West" type air masses is incompatible with long-range transport in the free troposphere and can be explained by the influence of a surface

ACPD
14, 9275–9343, 2014

circulation from the Gulf of Lyon and the Ligurian Sea triggered by the main westerly synoptic flow. This also means that the aerosol collected during the "West" regime was not necessarily more "aged" than those sampled in "PoV" air masses.

During the last two days (11–12 July), following the end of the westerly circulation and the reestablishment of continental air masses, seasalt concentrations decreased and the size-segregated chemical composition was characterized again by high fine-mode concentrations of secondary species and organic compounds. However, when compared to the composition characteristics of the first week, the daytime concentration of ammonium nitrate on 11–12 July was very small, and at night the nitrate size-distribution did not peak in the 0.42–1.2 µm size range but was rather equally distributed between the small (0.14–0.42 µm) and large (0.42–1.2 µm) accumulation mode size intervals. In general, the shape of the size-distribution on 11–12 July, with a less distinct peak in the large accumulation mode size range with respect to the composition observed during the first week of the campaign, is characteristic of a less processed aerosol.

In summary, the first week was characterised by submicron aerosols rich in water-soluble organic compounds, ammonium nitrate and sulphates, slowly accumulating over time. After the passage of a frontal system which cleaned the atmosphere, westerly conditions increased sea salt concentrations. A composition dominated by submicron organic matter and ionic species was found again in the last days of the experiment, but with an aerosol size-distribution showing a greater contribution of water-soluble organic and inorganic species (e.g. nitrate) in small particles ($D_p < 0.4$ µm) with respect to the first, more polluted, week of the campaign when large accumulation mode particles ($0.4 < D_p < 1$ µm) dominated the aerosol mass size distribution.

3.5 Submicron aerosol chemical composition from HR-ToF-AMS and SP-AMS

The HR-ToF-AMS was online 80 % of the time during the experiment (Fig. 4), while the SP-AMS measurements covered only the second part of the study (6–12 July). Absolute concentrations for the chemical compounds determined by the SP-AMS are

ACPD
14, 9275–9343, 2014

not discussed in this study as the instrument was uncalibrated, therefore only relative concentrations are discussed. The pie charts in Fig. 5 summarizes the PM_1 chemical composition from HR-ToF-AMS for the whole campaign and for the measurement period covered by the SP-AMS. The average chemical composition from SP-AMS is also shown for the same period. HR-ToF-AMS is insensitive to black carbon, so that BC mass concentrations were derived from the PSAP using a MAC of $10\,m^2\,g^{-1}$. The mass balance of PM_1 from HR-ToF-AMS shows a composition typical for polluted rural sites (Jimenez et al., 2009) with about a half of the mass accounted for by carbonaceous material and a nitrate/sulphate ratio exceeding 0.6. Similar proportions are found in the second part of the study (6–12 July), except for a smaller amount of BC. In the same period, the SP-AMS composition provides a very different picture, with a much greater contribution of BC but also of organic matter to the total analyzed mass. The nitrate-to-sulphate ratio is also higher (~ 0.9) from the SP-AMS than from the HR-ToF-AMS. As mentioned above, the SP-AMS concentrations were uncalibrated; however, we can assume that the measured refractory BC is equivalent to the BC estimated from the PSAP ($0.40\,\mu g\,m^{-3}$ on average) assuming a value of MAC of $10\,m^2\,g^{-1}$ then the total SP-AMS mass would amount up to one third of the mass concentrations from the HR-ToF-AMS, with a higher fraction for organic matter (38 %) than for nitrate (19 %) and sulphate (15 %).

When comparing the time trends of the concentrations of the main aerosol components measured by both HR-ToF-AMS and SP-AMS, very good correlations are found: $r^2 = 0.69$ (organic matter), 0.82 (nitrate), 0.65 (sulphate), 0.68 (ammonium), indicating that the BC-containing aerosols measured by the SP-AMS contribute significantly to the bulk non-refractory component mass concentrations determined by the HR-ToF-AMS. However, there were slight differences in the time trends of the specific components between the two instruments (Fig. 6). It can be observed, for example, that the concentration ratio between the HR-ToF and the SP for nitrate on 6 and 7 July was twice that on 10 to 12 July. This would suggest that the chemical composition and not a systematic instrumental source of error is responsible for the nitrate differences. In

ACPD
14, 9275–9343, 2014

this specific case, apparently on the first two days (6 and 7 July) nitrate was less internally mixed with BC than in the last days of the campaign. The modifications of the HR-ToF-AMS chemical composition following the changes in air mass type can be followed in Fig. 4a. The main features reflect the observations from the Berner impactor samples: submicron nitrate is strongly reduced during the days of westerly air masses; organic matter also exhibits higher concentrations during days of continental (PoV) air masses, with an increasing trend during the first week of the campaign (from 28 June to 5 July) explained by the accumulation of pollutants in the PBL under stagnant conditions. The high-time resolution allows examination of the daily cycles of the main chemical components (Fig. 7b): nitrate concentrations peak at 4–5 a.m. when RH is highest; sulphate trend is rather flat but with a relative maximum during the day-time, between 10 a.m. and 5 p.m.; organic matter diurnal trend shows two maxima, the main one during night-time (between 10 p.m. and 6 a.m.), and a second one around midday concomitant with that of sulphate. These maxima can be interpreted as due to condensation of semi-volatile components into the aerosol at night (previously reported by Dall'Osto et al., 2009) and photochemically related formation of SOA respectively. Interestingly, the AMS nitrate concentrations are very small in daytime (between 9 a.m. and 9 p.m.), in contrast with the results for submicron particles from Berner impactors and from ATOFMS, showing several days with non negligible concentrations in daytime (Fig. S6). The reason for such discrepancy cannot be fully clarified but it may be due to the different cut-offs used for the above instruments. An alternative explanation could be that submicron nitrate was partially present as non-volatile salts (potassium or calcium salts) for which the AMS is poorly sensitive. Such explanation, however, is not supported by the Berner impactor measurements indicating that potassium and alkaline metals accounted for only 5 % of the cation equivalent concentrations in PM_1.

3.6 Aerosol single-particle analysis by ATOFMS

The TSI ATOFMS provided good measurement coverage during the experiment (Fig. 4a and b). About 55 000 single particle mass spectra were collected. ART-2a

ACPD
14, 9275–9343, 2014

cluster analysis was performed on the ATOFMS dataset (Song el at., 1999; Dall'Osto and Harrison, 2006), and eight main particle types were found. Four additional particle types were found but were only present as spike events on selected days. There were 12 particle types in total. Table 1 summarises the frequency of the eight main particle types, and the relative mass spectra can be seen in Fig. 5. These eight particle types are described as:

- *EC: elemental carbon.* The mass spectrum shows strong peaks due to elemental carbon (C_n, m/z 12, 24, 36, 48, 60). This particle type has an aerodynamic diameter (D_a) of about 700 nm (accumulation mode) and is the typical particle seen for aged, "regional" aerosol. To make clear the difference from small BC particles from fresh emissions, this particle type will be called *EC-Reg* hereupon. Because of the selectivity of ATOFMS for black carbon, such particles must be considered as particularly enriched in EC instead of being pure EC. On the contrary, it is expected that 700 nm particles contain secondary inorganic and organic species, which are, however, less prominent in this particle cluster than in the NIT-Reg and SUL-Reg types described below.

- *EC-NIT: elemental carbon + nitrate.* Strong peaks due to nitrate (m/z −46 [NO_2], m/z −62 [NO_3]) are observed along with those of EC. This particle presents a D_a of about 700 nm, similarly to the EC cluster. This particle cluster corresponds to the "regional nitrate" detected in London during the study of Dall'Osto et al. (2009) and will therefore be named *NIT-Reg* hereon.

- *K-NIT: potassium + nitrate.* This particle type is characteristic of nitrate aerosol unmixed with EC. The peak at m/z 39 can be due to potassium, although previous studies (Dall'Osto et al., 2009) suggested that an organic contribution may be present depending on the m/z 39/41 ratio. K-NIT is less RH-dependent than NIT-Reg (see below) and also presents a smaller D_a at about 400–500 nm. This particle type was associated more with "local" nitrate in Dall'Osto et al. (2009) with

ACPD
14, 9275–9343, 2014

a finer mode, less aged, and less volatile than regional nitrate, and will be referred as *NIT-Local* in the following discussion.

– *EC-SUL: elemental carbon + sulphate.* This particle type also had a smaller D_a than NIT-Reg, at about 500 nm, and was seen mainly during day-time. The NIT-Reg and EC-SUL diurnal trends are clearly anticorrelated (Fig. 7a), with EC-SUL concentrations peaking in the afternoon hours. Such behaviour, already observed by Dall'Osto et al. (2009) in London, was attributed to the effect of the diel cycle of nitric acid condensation/evaporation on the same particle type: during night-time this regional particle type is seen with nitrate, which evaporates during day time leaving a smaller aerosol core composed of EC and sulphate. We again suggest EC-SUL as the core of NIT-Reg particles, and we will label it "*SUL-Reg*" in the following discussion.

– *NaCl: sodium chloride*, with mass fragments from Na (m/z 23), Na_2Cl (m/z 81) and a lesser peak from Cl (m/z −35). The mass spectrum also exhibits nitrate peaks (m/z −46 and m/z −62) reflecting the reaction between NaCl and HNO_3 and the displacement of chloride by nitrate.

– *K-CN-amine: potassium + organic nitrogen with amines.* This particle type is smaller than NIT-Reg with a D_a of about 550 nm. A strong peak at m/z 39 is seen in the positive mass spectra, due to potassium (K) or unidentified OC components. This particle type was found also internally mixed with organo-nitrogen species (m/z −26 and m/z −42, due to $[CN]^-$ and $[CNO]^-$, respectively). The strong peak at m/z 59 ($[N(CH_3)_3]^+$) is recognized as the dominant peak for trimethylamine (TMA) since it could not be produced from any other common amine species in previous laboratory studies (Angelino et al., 2001). This particle type was found internally mixed with nitrate and sulphate.

– *K-EC-NIT: potassium + elemental carbon + nitrate.* This particle type is characterized by small particles of about 450 nm and by a spectrum which is a hybrid

ACPD
14, 9275–9343, 2014

between those of NIT-Local and NIT-Reg: the major peaks are at m/z 36 (EC), m/z 39 (K, OC), nitrate (m/z −46, m/z −62). This cluster will be referred as *NIT-Local/Reg* hereupon.

– *OC-NIT-SUL: organic carbon + nitrate + sulphate.* This cluster presents a unique positive mass spectrum (Fig. 5d), with strong peaks at m/z 27 $[C_2H_3]^+$ and m/z 43 $[(CH_3)CO]^+$ usually associated with oxidized secondary organic aerosol, and m/z 51 $[C_4H_3]^+$, 63 $[C_5H_3]^+$, 77 $[C_6H_5]^+$ and 91 $[C_7H_7]^+$ which are indicative of a strong aromatic signature (McLafferty, 1993). The strong signals at m/z 29 $[C_2H_5]^+$ and m/z 41 $[C_3H_5]^+$ confirm the strong hydrocarbon-like signature. The particle size distribution of this cluster is bimodal with peaks at about 400 and 600 nm. When plotting the temporal trend of the two different size modes, there are no observed differences.

Most of the ATOFMS particle types are clearly more abundant during the first week of the experiment, when PoV air masses prevailed (Fig. 4a and b). EC-Reg particles concentrations slowly accumulated over time (until the 5 July storm), suggesting an advection to the site in recirculated PBL air. A similar day-by-day increasing trend of black carbon atmospheric concentrations during the first week of the study is also evident in the BC data from PSAP (Fig. S5b). This explains why ATOFMS attributes EC to large (aged) particles.

NIT-Reg concentrations are also highest during the first part of the study in connection with PoV air masses, but, contrary to EC-Reg, their diurnal trend shows concentration peaks during the night/morning hours when relative humidity is highest (Fig. 7a). Both maximum (nocturnal) and minimum (midday) concentrations of NIT-Reg increased from 29 June to 5 July, indicating an effect from accumulation of recirculated pollutants, similarly to the EC-Reg particles.

By contrast, the second week was characterised by much lower concentrations of the "regional" components (EC-Reg, NIT-Reg and SUL-Reg). NaCl particles were seen mainly during 9–11 July under "West" marine air masses, with a very good correlation

ACPD
14, 9275–9343, 2014

with the time trends of seasalt concentrations determined on the Berner impactors (r^2 = 0.95). With regard to nitrate containing particles, the second part of the field study was characterised by somewhat more sustained concentrations of the small nitrate-rich particles (NIT-Local). In addition, during the first part of the study, the ratio of regional nitrate to local nitrate is about three, whereas during the second part of the study the ratio is about one. These results are in line with those of the Berner impactors, showing that during the last days of the campaign, submicron nitrate was associated with smaller particles than during the first week of the study (Fig. S6). Clearly, the last days of the experiment (11–12 July) were less affected by regional sources of nitrate aerosols with respect to the first, more polluted week of the campaign. We hypothesize that in the last days there was not enough time to form the large (0.42–1.2 µm) nitrate-rich accumulation mode particles which characterized the first, more polluted period of the campaign.

EC-Reg, NIT-Reg, NIT-Local, SUL-Reg and NaCl were also found in a very different environment, during the REPARTEE campaign in London (Harrison et al., 2012), and provide therefore evidence that such ATOFMS particle populations can be common over vast European regions. The other four additional particle types found in this study account for smaller contributions to the particle loading at SPC (Table 1). The K-CN-amine particle type shows a peak at about 6–9 p.m., and mainly during 2–4 July with specific Po Valley trajectories (PoV WNW). The NIT-Local/Reg particle type exhibits a mass spectrum which is a mix between those of NIT-Local and NIT-Reg, however its time trend shows a maximum at the very beginning of the experiment (27–29 June) under PoV N air mass trajectories. The diurnal trend for organic particles mixed with secondary inorganic species (OC-NIT-SUL) exhibits a nocturnal maximum, but without an early morning peak, i.e., without any clear enrichment effect from enhanced relative humidity conditions. Its concentrations around midday always go to zero and there is no evidence of day-by-day accumulation during the first week of the campaign, meaning that these particles are mainly produced from local (Po Valley) sources without being efficiently recirculated in residual layers. The relative "fresh" nature of these organic

ACPD
14, 9275–9343, 2014

aerosol type is witnessed by the fact that the concentrations observed during the latest days of the campaign are comparable with those of the first (more polluted, with enhanced stagnation) week, dissimilarly to the NIT-Reg and EC-Reg types. However, the inorganic ionic material (nitrate, sulphate) internally mixed with organic compounds in these particle types indicate that such particles, despite being formed from local sources, are subjected to a fast atmospheric processing including the uptake of secondary compounds by gas-to-particle conversion.

3.7 Organic composition from PMF-AMS

In the sections above we have discussed concentrations and variability of the main inorganic aerosol components, organic matter and black carbon as well as their mixing state. The present section deals with organic compound composition and organic source apportionment.

3.7.1 HR-ToF-AMS PMF

Insight into the nature and origin of submicron organic aerosol (OA) was provided by positive matrix factorization (PMF) of AMS datasets (Ulbrich et al., 2009). PMF was run on both low and high resolution HR-TOF-AMS organic matrices. We present the spectra from a five factor solution for HR AMS (Fig. S7). This solution was validated by correlations with external factors (total r^2 with several ATOFMS species were higher).

– *HOA: hydrocarbon-like OA.* Comprising 14 % of OA, this factor contains the typical Hydrocarbon-like primary organic aerosol dominated by organic fragments for saturated hydrocarbons $[C_nH_{2n+1}]^+$ (m/z 29, 43, 57, 71) and unsaturated hydrocarbons $[C_nH_{2n-1}]^+$ (m/z 27, 41, 55, 69, 83). This factor is very similar to previously reported reference spectra of primary organic aerosol emitted from gasoline and diesel combustion sources (Canagaratna et al., 2004; Aiken et al., 2009).

ACPD
14, 9275–9343, 2014

– *COA: "Cooking" OA.* Comprising 8 % of OA, this spectrum is similar to the cooking aerosol seen in previous published studies (Allan et al., 2010; Mohr et al., 2012). Additional unique feature among all factors is having m/z of 41 ($[C_3H_5]^+$) as a clear hydrocarbon peak. The second strongest $[C_xH_y]^+$ peak can be seen at m/z 55 ($[C_4H_7]^+$), as well as m/z 67 ($[C_5H_7]^+$). However, oxidized organic carbon peaks can also be seen. The m/z 43 is mainly composed of its oxidized fraction ($[C_3H_2O]^+$) as well as the presence of a strong signal at m/z 44 ($[CO_2]^+$).

– *SV-OOA: semivolatile-OOA.* Comprising 17 % of OA, we use the terms "LV-OOA" (LV Low Volatile) and "SV-OOA" (SV Semi Volatile) as introduced by Jimenez et al. (2009) although we did not explicitly measure the volatility of the compounds within this study. LV-OOA and SV-OOA factors serve as a basis set for describing the range of physicochemical properties occurring in the dynamic evolution of OOA (Jimenez et al., 2009). The MS of this component is clearly characterized by prominent $C_xH_yO_z$ fragments, especially CO_2^+ (m/z 44), indicating presence of substantial amount of oxidized organic compounds.

– *LV-OOA-LO: low-volatility-OOA-less oxidized.* Comprising 22 % of OA, this factor has a very similar spectra to OOA regional, but the peaks at m/z 28 and 44 are less intense relative to other ions. We interpret this as less aged OOA. This can be also seen in Fig. 10c, where it is clear that LO presents a higher CH signature (m/z 15, m/z 27).

– *LV-OOA-MO: low-volatility-OOA-more oxidized.* Comprising 42 % of OA, this factor displays a strong m/z 28 and 44, as is typical of highly aged OOA as measured by AMS. The mass spectrum of LV-OOA-MO illustrates a dominant peak at m/z 44 ($[CO_2]^+$), similar to the more oxidized LV-OOA component determined at other urban sites (Lanz et al., 2007; Ulbrich et al., 2009; r^2 = 0.9).

Figures 9 and 7c show the temporal trends and the diurnal profiles of HR-ToF-AMS organic species. LV-OOA-MO is found during the first part of the study, like the EC-Reg

ACPD
14, 9275–9343, 2014

ATOFMS particle type, whilst the contribution of the less oxidised LV-OOA-LO is relatively larger during the second part of the study. This is consistent with the ATOFMS findings indicating a first week with more aged aerosol (rich of EC-Reg, NIT-Reg) and second week with more fresh particles (more NIT-Local). The diurnal profiles of both LV-OOA factors are similar to that of sulphate, with a maximum during day-time, whereas SV-OOA concentrations peak during night-time and early morning, similarly to nitrate as has been seen previously (Lanz et al., 2007; Jimenez et al., 2009; Mohr et al., 2012). HOA and COA are both enhanced during night-time, but they also show additional marked spikes at 8–10 p.m. (COA) and 9–11 p.m. (HOA). The diurnal profile of COA does not present the peak around lunch-time which was found in earlier PMF-AMS studies in urban areas (Allan et al., 2010; Mohr et al., 2012). On the other hand, similar diurnal trends, with an evening peak, were observed for food cooking aerosols in Riverside, California, employing GC/TAG techniques (Williams et al., 2010).

The emerging picture is in line with previous PMF-AMS analysis of the sources of OA in continental polluted sites: (a) primary OA (HOA and COA) accumulate overnight because of the reduced atmospheric mixing and dispersion; (b) HOA concentrations follow those of NO_x ($r^2 = 0.51$) pointing to traffic sources; (c) SV-OOA accumulates at night-time, with concentrations depending not only on source strength and transport but also on temperature, which explains the correlation with inorganic semivolatile compounds ($r^2 = 0.60$ with ammonium nitrate). Finally (d), the most oxidized factors (LV-OOA types) are characteristic of daytime conditions, when photochemical production of SOA and the entrainment of aged aerosols are greatest. We examined the correlation of AMS LV-OOA (MO+LO) with odd oxygen ($O_x = O_3 + NO_2$) (Fig. S9) (Wood et al., 2010). The correlation is only weakly positive ($r^2 = 0.12$). The main difference between O_x and OOA is that concentrations of the former drop at night as an effect of dry deposition. In other words, ozone does not behave like aerosols, and this poses a limit to the application of this proxy. In daytime, the concentrations of LV-OOA are more closely related to that of ozone ($r^2 = 0.27$), indicating that the maximum observed for the oxi-

ACPD
14, 9275–9343, 2014

dized OOAs between 10 a.m. and 5 p.m. is associated with the production/entrainment of photochemical products.

In Table 2, we report the correlation coefficients (as r^2) between the concentration time trends of the HR-ToF-AMS factors and chemical components and those of the ATOFMS clusters. The concentration of AMS organic matter is correlated with many ATOFMS clusters, suggesting that, even if organic fragments were found for only a few specific clusters, organic matter was actually internally mixed in several ATOFMS particle types, although ATOFMS was relatively insensitive to them, especially in the case of clusters NIT-Reg and NIT-Local/Reg. Particle types containing EC and showing a nocturnal accumulation (NIT-Reg) exhibit a correlation with AMS HOA, in agreement with a primary origin of hydrocarbon-like compounds from combustion sources in the Po Valley. A unique ATOFMS OC-NIT-SUL with a strong m/z 55 correlates well with SV-OOA and the COA (whose spectrum also shows a m/z 55 fragment). Organic particles internally mixed with sulphate like OC-NIT-SUL are compatible with the hypothesis of formation from condensation of semivolatile organics (SV-OOA) onto pre-existing particles during the cold hours of the day. At the same time, the correlation of COA with OC-NIT-SUL, which represents a particle type *not* containing EC, is compatible with the origin of cooking aerosols, which are emitted by thermal processes at temperatures that are too low to produce elemental carbon.

The LV-OOA-MO factor shows a positive correlation with ATOFMS particles types (NIT-Reg, EC-Reg, SUL-Reg) whose concentration time trends reflected an accumulation in the daytime PBL during the first week of the campaign, in agreement with our interpretation that the above three ATOFMS clusters were influenced by aged aerosol ("regional") sources.

3.7.2 SP-AMS PMF

The PMF- SP-AMS is less standardized than PMF for the HR-TOF. We present here a four factor solution obtained by processing the SP-AMS spectra recorded for organic matter + BC between 5 and 12 July (Figs. 7d and S8):

ACPD
14, 9275–9343, 2014

– HOA (16 % of OM) internally mixed with BC, typical signature of strong m/z 43 and m/z 57, strong BC signature. Nitrogen-containing fragments (m/z 73 and m/z 58) are also visible and can be attributed to amines.

– OOA-Night (38 % of OM), with strong peaks at m/z 43, 55, 69, 81. The spectrum is reminiscent of that of the SV-OOA from HR-ToF-AMS, or a more oxidised traffic related anthropogenic signature. It was observed mainly during night time but showing sustained concentrations also in the early morning, consistent with semivolatile compound behaviour (Fig. 7d).

– OOA-Day (29 % of OM), with a very different spectrum with respect to OOA-Night and also an opposite diurnal trend (Fig. 7d). The OOA-Day signature includes many more oxygenated fragments (red), reminiscent of the spectrum of a LV-OOA. Characteristic fragments are: m/z 39, 41, 55 series, and a unique m/z 31, 45, 85, 99, 111 attributable possible to ethers or saturated carbonyls (McLafferty et al., 1993), although this should be confirmed with laboratory studies currently not been carried out with SP-AMS.

– LV-OOA (17 % of OM), typical OOA, the most oxidised one. Its diurnal trend is flat (Fig. 7d), indicating a well-mixed, most aged OA.

The fact that PMF finds fewer factors in the SP-AMS dataset than from the HR-ToF can be attributed to the fact that the SP-AMS record is shorter, therefore it contains less variance. For this reason, beside the good correlation between the HOAs extracted from the two datasets (r^2 = 0.45), attributing the SP-AMS factors to the HR-ToF-AMS factors is challenging. But one evident difference is that organic matter measured by SP-AMS seems to be less contributed by LV-OOA types of organics than the OA ionized in the HR-ToF-AMS, which may indicate that a substantial fraction of the HR-ToF LV-OOA is externally mixed with BC, although it may also be that the decarboxylation process responsible for the characteristic OOA mass spectrum during normal AMS vaporisation does not occur in the same manner in the SP-AMS. Furthermore, the

ACPD
14, 9275–9343, 2014

vapours may be detected in the SP-AMS at different effective relative ionisation efficiencies (RIEs). In fact, the HR-ToF LV-OOA-MO correlates better with the SP-AMS OOA-Day (r^2 = 0.65) than with the SP-AMS LV-OOA.

3.8 Organic speciation from HR-ToFMS-TAG

Organic marker information was provided by HR-TofMS-TAG during the last days of the campaign (7–11 July). This was the first field deployment of a TAG system adapted to a TofWerk HR-ToFMS detector, which later led to the development of a combined TAG-Aerosol Mass Spectrometer (Williams et al., 2014). During operation at SPC, the HR-ToFMS-TAG incorporated a custom heated transfer line between the GC and ToFMS, and a high pass quadrupole filter to eliminate carrier gas (helium) ions prior to ToFMS detection. TAG chromatograms were directly inserted into a PMF analysis using a novel chromatogram binning technique (Zhang et al., 2014). A 20-factor solution was used to separate the complex chromatograms. Several of the factors resulted from factor splitting, and were recombined to compare with AMS and ATOFMS factors. Several factors are a result of thermal decomposition as evidenced by the early GC retention time. The main categories of HR-ToFMS-TAG PMF components include:

- *alkanes*: (2 factors), one alkane factor is representative of an Unresolved Complex Mixture (UCM), likely composed of many straight- and branched- alkanes,
- *benzoic acid*,
- *monocarboxylic acids*: (2 factors), one monocarboxylic acid factor has a contribution from thermal decomposition at the start of chromatograms,
- *organic nitrogen:* (2 factors), containing ions such as m/z 30 and 46,
- *sulphate/organosulphate:* containing ions such as m/z 48 and 64,
- *chloride-containing:* containing ions such as m/z 36,

ACPD
14, 9275–9343, 2014

- *unknown decomposition products:* (6 factors), large contribution at beginning of chromatograms,
- *unknowns:* (4 factors), unidentified factors that contribute little to the total ion signal,
- *column bleed:* GC column bleed typical of chromatography.

See Supplement for a complete list of TAG PMF factors, factor profiles (Fig. S11), and their correlations to AMS PMF factors and ATOFMS clusters (Table S2).

Figure 10 reports the time trends of the total concentrations of the three main classes of compounds along with the time series of external tracers (AMS and ATOFMS factors) with aim of comparison. Clearly, alkanes correlated with the AMS HOA, as expected, but also with ATOFMS EC and EC-NIT (NIT-Reg), and finally with BC from PSAP, all correlations supporting an origin of alkanes from primary combustion sources. Benzoic acid (Fig. 10b) concentrations correlate with those of LV-OOA-MO, providing direct evidence that the aerosols characteristic of day-time conditions, containing sulphate and most oxidized LV-OOA, had significant contributions from photochemical products of anthropogenic origin. Benzoic acid has been shown in previous studies to correlate with anthropogenic SOA (Williams et al., 2010). Finally, monocarboxylic acids (Fig. 10c) show a positive correlation with AMS COA, which is consistent with the hypothesis of a prevalent source from food cooking. Monocarboxylic acids have been found to correlate well with food cooking sources during previous deployments of the TAG system (Williams et al., 2010).

In summary, the TAG analysis supports the previous interpretations of the AMS and ATOFMS factors, at the same time providing unambiguous information on the possible anthropogenic vs. natural sources.

ACPD
14, 9275–9343, 2014

3.9 Water-soluble organic composition from H-NMR analysis

NMR data were available at low time resolution (12 h) and refer to the water-soluble fraction of OAs. Recently, factor analysis was tested on atmospheric NMR datasets for organic source apportionment (Finessi et al., 2011; Paglione et al., 2013). Here we present the results for the 2009 Po Valley campaign with the aim of comparison with PMF-AMS.

PMF and two other factor analysis algorithms (see experimental section) were applied to the NMR datasets emerging from the analysis of the 12 h resolution filters. The 4-factor solution was the simplest one for which the three algorithms showed consistent results for both contributions and profiles. Figure 11 shows the spectra of the four factors:

- *Factor 1:* This factor is composed of aliphatic amines and unspeciated aliphatic compounds, and mainly occurs at night-time. Speciated amines include DMA (dimethyl-), TMA (trimethyl-), DEA (diethyl-), TEA (triethyl-amine) are present in this factor.

- *Factor 2:* This factor is composed of aliphatic alkanoic acids and oxo-acids (i.e., compounds characterized by linear chains with or without terminal methyls and oxo- or carboxyl substitutions). Although these compounds contribute in trace amounts and are also present in blanks and back-up filters, we believe these are genuine aerosol components, as concentrations are much higher in the sampled (front) filters.

- *Factor 3 and Factor 4:* These factors have spectral profiles characterized by the broad bands of polysubstituted aliphatic compounds with some aromatics, as expected for "humic-like substances" (HULIS) (Graber and Rudich, 2006). Both exhibit broad resonances in the range of the alkyl and substituted alkyl functional groups with very few specific peaks with the exception of that of MSA in the case of F3 (singlet at 2.81 ppm). F4 shows greater amounts of alkoxy (HC-O) groups and

ACPD
14, 9275–9343, 2014

of aliphatic groups highly substituted by oxo or carboxyl groups (region around 2.6 ppm) and lesser amounts of terminal methyls (0.9 ppm) with respect to F3.

The comparison of time trends of the four WSOC factors with inorganic tracers and BC is summarized in Table 3. No factors correlate with seasalt. The best correlations are found for Factor 1 and ammonium nitrate and black carbon, and between the HULIS factor F4 and nss-sulphate. These findings indicate that Factor 1 originates from anthropogenic sources in the nocturnal boundary layer and that at least one of the HULIS factors is mainly of secondary origin from regional sources. Interestingly, BC shows positive correlations with both non-HULIS factors (F1 + F2, mainly driven by F1) and with the composite HULIS factor (F3 + F4), suggesting that combustion sources contributed to WSOC both at night-time and in daytime conditions. Indeed the examination of BC time trends from PSAP (Fig. S5b) indicates the presence of two components: one associated with fresh emissions in the nocturnal stable layer, and a second one associated with the day-by-day accumulation in residual and mixing layers. Finally, the positive correlation of HULIS F4 with SO_2 is due to the tendency of very oxidized organic aerosols to show relative maxima in concentrations during daytime in the same manner as SO_2, and also because of the greater HULIS levels in air masses having a continental component ("PoV" from W, N and E sectors) with respect to air masses with a marine component.

When comparing the PMF-AMS results with those emerging from NMR factor analysis, one should keep in mind that the latter was applied only to the water-soluble fraction of submicron aerosol organic compounds. For this reason, HOA should not be accounted for by the NMR characterization. We have contrasted the time trends of NMR and (time-integrated) AMS factors and plotted in Fig. 12a. The figure shows a good fit for AMS LV-OOA-LO (less oxidised) with NMR F3 (HULIS with MSA) ($r^2 = 0.49$) and a discrete fit of AMS SV-OOA with NMR F1 (amine and aliphatic) ($r^2 = 0.45$). The best correlation is found between AMS LV-OOA-MO and NMR HULIS F4 ($r^2 = 0.65$) although the AMS factor concentrations are greater. The correlation of COA with NMR factors is weak. During the second part of the campaign, the concentrations of COA

ACPD
14, 9275–9343, 2014

tend to follow those of NMR F2 (alkanoic acid, $r^2 = 0.75$ after 5 July). A better match can be obtained by aggregating factors (Fig. 12b, Table 4), showing that there is a good overlap between the AMS total LV-OOA (composite of -LO and -MO) and the NMR "HULIS" (F3 + F4). This picture also shows that NMR F1 + F2 are linked to the AMS SV-OOA + COA. Therefore, a clear split between OOA components forming from surface sources in the Po Valley (SV-OOA + COA ∼ NMR Factors 1, 2) and those characterizing background air and correlating with sulphate (LV-OOAs ∼ NMR factors 3, 4) is supported by the combination of the two spectroscopic techniques.

As a final remark, if we assign NMR HULIS to AMS LV-OOAs and NMR Factor 1 (amines) to AMS SV-OOA, then a correspondence between NMR Factor 2 (alkanoic acids) and AMS COA can be postulated. Alkanoic acids can actually form from oxidation of oleic acids and are commonly formed by meat cooking and food frying (Abdullahi et al., 2013), and likewise these includes monocarboxylic acids found by the HR-TofMS-TAG (see Sect. 3.8).

4 Discussion

4.1 Evolution of aerosol mixing state

The above survey of the aerosol mass spectrometer observations together with the organic characterization from TAG and NMR exemplifies the complexity of the chemical processes governing the evolution of composition and mixing state of the aerosol at a polluted continental site. It also shows that during the period of stagnant "PoV" air masses, such processes are mainly triggered by the diurnal variability in the intensity of photochemistry and of atmospheric mixing as well as in the basic thermodynamic parameters (T, RH). As a consequence, two different regimes of aerosol formation can be identified (Fig. 13): (a) at night-time in the nocturnal surface layer (≤∼ 500 m a.s.l.), and (b) in daytime when processed aerosols are entrained from air layers aloft (500–2000 m a.s.l.).

ACPD
14, 9275–9343, 2014

At night-time, due to the reduced mixing height, the aerosol composition is directly impacted by the emissions of primary particles from ground sources in the Po Valley and by the condensation of inorganic and organic secondary materials promoted by the cold and humid conditions. As a result of the emission of primary particles, some containing BC (like the combustion particles rich of HOA), some unmixed with BC (like the COA), a complex aerosol mixing state is seen by the ATOFMS (step "1" in the figure). Particle types very rich in BC (the ATOFMS "EC-Reg" type), moderately rich in BC ("NIT-Reg") and with no EC (NIT-Local and OC-SUL-NIT) were in fact observed. The poorly oxidized organic compounds entering the aerosol under these conditions include the alkanes identified by TAG, the amines determined by H-NMR, and the alkanoic acids identified by both TAG and H-NMR.

During the day, the drop in RH, the temperature increase and the dilution of the aerosol in a deeper mixing layer leads to the evaporation of semivolatile inorganic (ammonium nitrate) and organic (SV-OOA, HOA and possibly COA) compounds while the condensation of new oxidized secondary compounds (such as the benzoic acid from TAG) takes place. As a result, the most common particle types rich in ammonium nitrate encountered at night-time and early morning (NIT-Reg) get denuded and the ATOFMS is able to ablate their ammonium sulphate + BC core (the "SUL-Reg"), although the very large NIT-Reg particles may survive evaporation and accumulate in the PBL at the regional scale (step "2"). The ATOFMS is probably insensitive to changes in coating of the particles very rich in BC (the "EC-Reg" type) (step "3"). During the day, the condensation of ammonium sulphate and of highly oxygenated SOA tends to reduce external mixing and a few particle types are observed by the ATOFMS. Since the secondary aerosols formed during daytime (i.e., photochemically) are not volatile, they tend to accumulate over time, and their mass ratio with respect to the primary components (such as BC) tends to increase (step "4"). As a consequence, a fraction of these particles are not seen or seen with slight sensitivity by both SP-AMS and ATOFMS. In daytime, particles are entrained from residual layers, including elevated layers bringing

ACPD
14, 9275–9343, 2014

aerosols that have experienced long-range transport (step "5"), and after sunset they are also exported in the residual layers (step "6").

The impact of these simple meteorological factors on aerosol dynamics was evident throughout the campaign except for the "West" air masses. However, even with continental air masses, the actual impact of the meteorological factors qualitatively depicted in Fig. 13 varied day by day following the changes in weather conditions (stagnation vs. more ventilation). In particular, during the first week of campaign, recirculation of aged aerosols (steps 2 to 6 in Fig. 13) was more important than during the last days of PoV air masses between 10–12 July, whereas the nocturnal production of fresh aerosols (step 1) occurred constantly on every day under PoV air masses, and consequently became relatively more significant on the last days. To summarize the effect of atmospheric transport conditions on aerosol mixing state, we have used indexes obtained by compacting the ATOFMS data into a few main categories: soot (EC-Reg), coated soot (i.e., soot mixed with non-refractory components) (NIT-Reg + SUL-Reg + NIT-Reg/local), purely non-refractory particles (i.e., unmixed with soot) (NIT-Local + K-CN-Amines + OC-SUL-NIT). We have then produced daily cycles of the concentrations of such particle populations separately for the first week (28 June–4 July) and for the last days of the experiment (10–12 July), when SP-AMS data were also available (Fig. 14).

Clearly, the concentrations of soot-containing particles were much lower in the end of the period than during the first week of more polluted conditions. The proportion of soot particles which was actually mixed with (or "coated" by) non-refractory compounds was generally high during the first polluted period (between 70 % and 90 %), with a maximum between 4:00 and 10:00 LT, which corresponds to time window when most of the nitrate-coated EC particles (NIT-Reg) were found. Nitrate condensation was certainly promoted by the high RH and low temperature before dawn, and possibly also sustained by the photochemical production of nitric acid for some hours after dawn when NO_x concentrations are still high (Fig. 1). The fraction of particles containing non-refractory compounds (OC, sulphate, nitrate) mixed with soot was 60–70 %

ACPD
14, 9275–9343, 2014

in the first week, whereas in the last days, such proportion was much lower and was noticeably small in evening hours (down to 20 %), possibly due to the production of POA from sources not emitting EC (like food cooking). Finally, we plotted the diurnal cycle of the total AMS mass of non-refractory compounds measured by the SP-AMS with respect to that measured by the HR-Tof-AMS. Because the SP-AMS concentrations are uncalibrated, we focus here only on the shape of the diurnal cycle of this ratio, which exhibits a maximum between 5:00 and 10:00 LT. Apparently, the morning peak in EC coating by nitrate (and organics?) observed by the ATOFMS is reflected by a greater proportion of compounds internally mixed with EC seen by the SP-AMS. The behaviour of these metrics for aerosol mixing state becomes more confused in the afternoon/evening, possibly because of the insensitivity of ATOFMS to some types of organic coatings on the large EC particles.

4.2 Effect of PBL meteorology on aerosol organic composition

The two regimes of aerosol formation schematically depicted in Fig. 13 imply two different source footprints: night-time–early morning aerosols, accumulating in the nocturnal surface layer or in an incipient mixing layer, must originate from ground-level sources at low elevation in the Po Valley basin (hence mainly anthropogenic), while the aerosol entrained in the middle of the day and afternoon hours can be impacted by sources much further away. We dedicate this final part of the discussion to investigate possible footprints for the oxidized secondary aerosols (and of recirculated primary aerosols) which dominate the composition in daytime.

Ozone and (at least partly) LV-OOA are photochemically formed, but the actual oxidation processes can occur in situ in the Po Valley sector enclosing the station, or elsewhere with the products being mainly transported to SPC. The lidar-ceilometer data suggest that aerosols in residual layers are clearly impacted by recirculation of particles (and of their precursors) lifted from ground-level sources during the mixing layer deepening on the day before. In order to test this hypothesis, we recorded the equivalent potential temperature θ_e in residual layers at 850 hPa (~ 1500 m a.s.l.), which can be

ACPD
14, 9275–9343, 2014

used to trace boundary layer air during the conditions of the experiment. Indeed, meteorological models and reanalysis data (ERA-interim) for typical summertime conditions over Italy clearly show that warm humid air is lifted to the 850 hPa level from the surface level in daytime through thermal convection amplified by orographic transport along the Apennines and the Alps ridges. Equivalent potential temperature data show that warm humid air persists overnight at 850 hPa, undergoes some transport according to wind regimes and can be eventually recirculated the day after. To investigate the effect of such atmospheric dynamics on the OOA concentrations in the rural Po Valley, we compared θ_e in residual layers in the night over SPC (from radiosoundings at 00:00 UTC) with the LV-OOA concentrations on the day after. We found a moderately positive correlation (r^2 = 0.38) (Fig. 15). The correlation is degraded by the sample of 5 July, when intense precipitation and aerosol scavenging occurred: on that day, a conservative behaviour cannot be assumed for water vapour nor for aerosols. If we omit this day, the correlation is much more robust (r^2 = 0.65). We can therefore safely state that LV-OOA are mainly associated with recirculated PBL air that had lifted over continental areas, rather then from transport in the free troposphere from very remote sources. To further investigate the possible extension of the footprint of the "regional" source footprint (the Po Valley? Europe?) of the LV-OOA, we report maps of θ_e obtained from ERA-interim for the great Alpine region and for North Italy in night-time hours and for specific periods of the campaign (Fig. S10). These will show the horizontal extension of residual layers influenced by boundary layer sources under varying meteorological regimes. From the first days of the campaign until 4 July, high nocturnal θ_e are found throughout the great Alpine region and neighbouring areas, which could act as source areas for the precursors of sulphate and SOA, especially in the very first days (28–29 June), when the main circulation was from north, i.e., from Central Europe and across the Alps. The intensification of convection with consequent lifting of PBL air in the region was observed progressively until 4 July and this corresponds to the increase of aerosol extinction observed by the ceilometer in these days. In the days of westerly flows (8 July is shown in the figure), the convection of warm humid air is completely switched

ACPD
14, 9275–9343, 2014

off in the areas north of the Alps, which are directly influenced by the fresh Atlantic air masses. Conversely, warm air persists over the Po Valley meaning that convection along the Apennines and over warm Mediterranean basins is still active. On 11 July, convection is strongly reduced almost everywhere and we observe in this day a general minimum of θ_e in residual layers. Notice that this is also the day showing minimum concentrations of odd oxygen (O_x) and of total LV-OOAs. On 12 July, we observe some recovery in the western sectors, but the Po Valley is influenced by an easterly flow, i.e., from areas where θ_e is still quite low. Now, the analysis of the temporal trends of the HR-ToF-AMS LV-OOA factors indicate that the *most oxidized* (LV-OOA-MO) are found on days characterized by continental air masses (from N like 28 June, NW like 3 July or E like 12 July) and in higher concentrations when also θ_e over Central Europe (the great Alpine region and neighbouring areas) is high. Conversely, the concentrations of *less oxidized* low-volatility OOA (LV-OOA-LO) recovery against those of LV-OOA-MO when convection starts intensively over the Po Valley (3 July), and especially during the days of westerly flow (8 July) when the source areas of PBL air in Central Europe are switched off, while convection (and lifting of gases and particles) is still active in North Italy and in the Ligurian Sea. These observations support the concept of the two classes of LV-OOA (and of NMR HULIS) representing two end-members of an atmospheric ageing process, with one more local and less processed, and another more regional and more processed. In particular, the LV-OOA-LO (and NMR F3) are associated with recirculated PBL air lifted over North Italy, while the LV-OOA-MO (and NMR F4) originate from PBL air lifted over a wider continental area encompassing the great Alpine region and Central Europe. The oxidation level can therefore be put in relation to the extent of transport. Indeed, the rise in concentration of the LV-OOA-LO during the first days of July until 4 July is concomitant with an increase of BC, suggesting that a fraction of LV-OOA can be considered "fresh" or "incipient", in the sense that if forms quite readily from local (Po Valley) emissions. Inversely, the LV-OOA-MO, which does not show any increase after atmospheric stability increases over North Italy around 1–

ACPD
14, 9275–9343, 2014

2 July can be considered as more influenced from sources outside the Po Valley and hence contributing to background concentrations.

Finally, the analysis of θ_e maps also provides an explanation for why the ratio between local and regional OOAs is *higher* in days where back-trajectories indicate a long-range transport in westerly air masses (8–9 July): on those days, convection and lifting of aerosol and precursors was strongly reduced at the regional scale. These results indicate that the classification of aerosols based on back-trajectory analysis should be done with caution in areas characterized by complex orography and boundary layer dynamics.

5 Conclusions

In this experiment we performed sophisticated investigations of the aerosol chemical composition and mixing state using modern aerosol spectrometers at a continental regional background site. Previous field experiments using analogous experimental approaches focused on environments characterized by a localized big urban source, or were performed at coastal sites where there is a consistent air flow from in-land large emission sites to the ocean (Chebogue Point, in the frame of NEAQS – ITCT). In such environments, it is possible to link aerosol composition to the travel time from the source areas (e.g., Doran et al., 2007). Most of the time, however, one measuring station can just be surrounded by anthropogenic and natural sources in any directions. Under such, more common, circumstances, the critical variables are the presence of geographical barriers (mountain ridges) and, most importantly, the height of the mixing layer, which in turns regulates the entrainment of aerosols transported in the elevated layers. We have shown in this study that anthropogenic aerosols can accumulate in geographical basins (like the Po Valley) in the presence of atmospheric stratification, but in typical summertime daytime conditions, with a 1500–2000 m thick PBL, transport can occur even across a tall mountain chain like the Alps. Our organic source apportionment results indicate that anthropogenic aerosols accumulating in the lower layers overnight

ACPD
14, 9275–9343, 2014

accounted for 38 % (HOA + COA + SV-OOA) of OA mass on average, while another 21 % was accounted for by more aged aerosols (LV-OOA-LO) recirculated in residual layers but still originating in North Italy, and finally a considerable fraction (41 %) was due to aged aerosols (LV-OOA-MO) from transalpine transport.

The dynamic of the PBL affects also the aerosol compounds mixing state. At evening/night, when the atmosphere was stratified, the impact from fresh, diverse primary emissions (traffic, possibly cooking) increased the extent of external mixing, but such an increase was only partially compensated by the condensation of semivolatile compounds (ammonium nitrate, amines) which took place in the coldest hours of the day (late night) and after dawn when photochemistry starts while NO_x concentrations are still high. During the day, the evaporation of particles made of semivolatile components and the condensation of photochemically produced non-volatile secondary compounds (highly oxidized SOA, sulphates) reduced the degree of external mixing, but the simultaneous entrainment of particles from residual layers introduced an additional element of complexity. Residual layers brought recirculated primary particles including black carbon aerosols. As a result, in the middle of the day only 75–80 % of the EC-containing particles measured by single-particle analysis were coated by non-refractory compounds (while early in the morning they were 90 %). In the last part of the campaign, which was less polluted and the black carbon concentrations small (0.2–0.6 $\mu g\,m^{-3}$), about half of the accumulation mode particles measured by the ATOFMS were unmixed with EC, i.e., made purely of non-refractory components. This finding contributes to the explanation of different chemical compositions measured by the SP-AMS and the HR-ToF-AMS. Overall, a full internal mixing between BC and the non-refractory aerosol chemical components was not observed during the experiment in this environment.

Supplementary material related to this article is available online at http://www.atmos-chem-phys-discuss.net/14/9275/2014/acpd-14-9275-2014-supplement.zip.

ACPD
14, 9275–9343, 2014

Acknowledgements. This work was funded by European integrated project on aerosol cloud climate and air quality interactions (No 036833-2, EUCAARI). The ERA-Interim data were kindly provided by Silvio Davolio (CNR-ISAC). Data analysis was co-funded by the project PEGASOS (EC FP7-ENV-2010-265148) and by the project SUPERSITO of Region Emilia-Romagna. ACCENT+ is also gratefully acknowledged. Finally, Emanuela Finessi (CNR-ISAC, now at University of York) is also gratefully acknowledged for the precious work in aerosol filter collection in the field. Manuel Dall'Osto and Roy M. Harrison thank the UK National Centre for Atmospheric Science for financial support. Work by Georg Stange, K. Michl and R. T. Wilhelm (all DWD) on gas phase constituents is greatly acknowledged.

References

Abdullahi, K. L., Delgado-Saborit, J. M., and Harrison, R. M.: Emissions and indoor concentrations of particulate matter and its specific chemical components from cooking: a review, Atmos. Environ., 71, 260–294, 2013.

Aiken, A. C., Salcedo, D., Cubison, M. J., Huffman, J. A., DeCarlo, P. F., Ulbrich, I. M., Docherty, K. S., Sueper, D., Kimmel, J. R., Worsnop, D. R., Trimborn, A., Northway, M., Stone, E. A., Schauer, J. J., Volkamer, R. M., Fortner, E., de Foy, B., Wang, J., Laskin, A., Shutthanandan, V., Zheng, J., Zhang, R., Gaffney, J., Marley, N. A., Paredes-Miranda, G., Arnott, W. P., Molina, L. T., Sosa, G., and Jimenez, J. L.: Mexico City aerosol analysis during MILAGRO using high resolution aerosol mass spectrometry at the urban supersite (T0) – Part 1: Fine particle composition and organic source apportionment, Atmos. Chem. Phys., 9, 6633–6653, doi:10.5194/acp-9-6633-2009, 2009.

Allan, J. D., Jimenez, J. L., Williams, P. I., Alfarra, M. R., Bower, K. N., Jayne, J. T., Coe, H., and Worsnop, D. R.: Quantitative sampling using an Aerodyne aerosol mass spectrometer – 1. Techniques of data interpretation and error analysis, J. Geophys. Res.-Atmos., 108, 4090, doi:10.1029/2002JD002358, 2003.

Allan, J. D., Delia, A. E., Coe, H., Bower, K. N., Alfarra, M. R., Jimenez, J. L., Middlebrook, A. M., Drewnick, F., Onasch, T. B., Canagaratna, M. R., Jayne, J. T., and Worsnop, D. R.: A generalised method for the extraction of chemically resolved mass spectra from aerodyne aerosol mass spectrometer data, J. Aerosol Sci., 35, 909–922, doi:10.1016/j.jaerosci.2004.02.007, 2004.

ACPD
14, 9275–9343, 2014

Allan, J. D., Williams, P. I., Morgan, W. T., Martin, C. L., Flynn, M. J., Lee, J., Nemitz, E., Phillips, G. J., Gallagher, M. W., and Coe, H.: Contributions from transport, solid fuel burning and cooking to primary organic aerosols in two UK cities, Atmos. Chem. Phys., 10, 647–668, doi:10.5194/acp-10-647-2010, 2010.

Angelino, S., Suess, D. T., and Prather, K. A.: Formation of aerosol particles from reactions of secondary and tertiary alkylamines: characterization by aerosol time-of-flight mass spectrometry, Environ. Sci. Technol., 35, 3130–3138, 2001.

Berresheim, H., Elste, T., Plass-Dülmer, C., Eisele, F. L., and Tanner, D. J.: Chemical ionization mass spectrometer for long-term measurements of atmospheric OH and H_2SO_4, Int. J. Mass Spectrom., 202, 91–109, 2000.

Bond, T. C., Anderson, T. L., and Campbell, D.: Calibration and intercomparison of filter-based measurements of visible light absorption by aerosols, Aerosol Sci. Tech., 30, 582–600, 1999.

Canagaratna, M. R., Jayne, J. T., Ghertner, D. A., Herndon, S., Shi, Q., Jimenez, J. L., Silva, P. J., Williams, P., Lanni, T., Drewnick, F., Demerjian, K. L., Kolb, C. E., and Worsnop, D. R.: Chase studies of particulate emissions from in-use New York city vehicles, Aerosol Sci. Tech., 38, 555–573, 2004.

Canagaratna, M. R., Jayne, J. T., Jimenez, J. L., Allan, J. D., Alfarra, M. R., Zhang, Q., Onasch, T. B., Drewnick, F., Coe, H., Middlebrook, A., Delia, A., Williams, L. R., Trimborn, A. M., Northway, M. J., DeCarlo, P. F., Kolb, C. E., Davidovits, P., and Worsnop, D. R.: Chemical and microphysical characterization of ambient aerosols with the aerodyne aerosol mass spectrometer, Mass Spectrom. Rev., 26, 185–222, 2007.

Carbone, C., Decesari, S., Mircea, M., Giulianelli, L., Finessi, E., Rinaldi, M., Fuzzi, S., Marinoni, A., Duchi, R., Perrino, C., Sargolini, T., Varde, M., Sprovieri, F., Gobbi, G. P., Angelini, F., and Facchini, M. C.: Size-resolved aerosol chemical composition over the Italian Peninsula during typical summer and winter conditions, Atmos. Environ., 44, 5269–5278, 2010.

Crosier, J., Allan, J. D., Coe, H., Bower, K. N., Formenti, P., and Williams, P. I.: Chemical composition of summertime aerosol in the Po Valley (Italy), northern Adriatic and Black Sea, Q. J. Roy. Meteor. Soc., 133, 61–75, 2007.

Dall'Osto, M. and Harrison, R. M.: Chemical characterisation of single airborne particles in Athens (Greece) by ATOFMS, Atmos. Environ., 40, 7614–7631, 2006.

Dall'Osto, M., Harrison, R. M., Coe, H., Williams, P. I., and Allan, J. D.: Real time chemical characterization of local and regional nitrate aerosols, Atmos. Chem. Phys., 9, 3709–3720, doi:10.5194/acp-9-3709-2009, 2009.

ACPD
14, 9275–9343, 2014

Dall'Osto, M., Querol, X., Alastuey, A., Minguillon, M. C., Alier, M., Amato, F., Brines, M., Cusack, M., Grimalt, J. O., Karanasiou, A., Moreno, T., Pandolfi, M., Pey, J., Reche, C., Ripoll, A., Tauler, R., Van Drooge, B. L., Viana, M., Harrison, R. M., Gietl, J., Beddows, D., Bloss, W., O'Dowd, C., Ceburnis, D., Martucci, G., Ng, N. L., Worsnop, D., Wenger, J., Mc Gillicuddy, E., Sodeau, J., Healy, R., Lucarelli, F., Nava, S., Jimenez, J. L., Gomez Moreno, F., Artinano, B., Prévôt, A. S. H., Pfaffenberger, L., Frey, S., Wilsenack, F., Casabona, D., Jiménez-Guerrero, P., Gross, D., and Cots, N.: Presenting SAPUSS: Solving Aerosol Problem by Using Synergistic Strategies in Barcelona, Spain, Atmos. Chem. Phys., 13, 8991–9019, doi:10.5194/acp-13-8991-2013, 2013.

DeCarlo, P. F., Kimmel, J. R., Trimborn, A., Northway, M. J., Jayne, J. T., Aiken, A. C., Gonin, M., Fuhrer, K., Horvath, T., Docherty, K. S., Worsnop, D. R., and Jimenez, J. L.: Field-deployable, high-resolution, time-of-flight aerosol mass spectrometer, Anal. Chem., 78, 8281–8289, 2006.

Decesari, S., Finessi, E., Rinaldi, M., Paglione, M., Fuzzi, S., Stephanou, E. G., Tziaras, T., Spyros, A., Ceburnis, D., O'Dowd, C., Dall'Osto, M., Harrison, R. M., Allan, J., Coe, H., and Facchini, M. C.: Primary and secondary marine organic aerosols over the North Atlantic Ocean during the MAP experiment, J. Geophys. Res., 116, D22210, doi:10.1029/2011JD016204, 2011.

Deserti, M., Savoia, E., Cacciamani, C., Golinelli, M., Kerschbaumer, A., Leoncini, G., Selvini, A., Paccagnella, T., and Ribaldi, S.: Operational meteorological pre-processing at Emilia-Romagna ARPA Meteorological Service as a part of a decision support system for air quality management, Int. J. Environ. Pollut., 16, 571–582, 2010.

Di Giuseppe, F., Riccio, A., Caporaso, L., Bonafè, G., Gobbi, G. P., and Angelini, F.: Automatic detection of atmospheric boundary layer height using ceilometer backscatter data assisted by a boundary layer model, Q. J. Roy. Meteor. Soc., 138, 649–663, doi:10.1002/qj.964, 2012.

Docherty, K. S., Stone, E. A., Ulbrich, I. M., DeCarlo, P. F., Snyder, D. C., Schauer, J. J., Peltier, R. E., Weber, R. J., Murphy, S. M., Seinfeld, J. H., Eatough, D. J., and Jimenez, J. L.: Apportionment of primary and secondary organic aerosols in Southern California during the 2005 Study of Organic Aerosols in Riverside (SOAR), Environ. Sci. Technol., 42, 7655–7662, doi:10.1021/es8008166, 2008

Doran, J. C., Barnard, J. C., Arnott, W. P., Cary, R., Coulter, R., Fast, J. D., Kassianov, E. I., Kleinman, L., Laulainen, N. S., Martin, T., Paredes-Miranda, G., Pekour, M. S., Shaw, W. J., Smith, D. F., Springston, S. R., and Yu, X.-Y.: The T1-T2 study: evolution of aerosol proper-

ACPD
14, 9275–9343, 2014

ties downwind of Mexico City, Atmos. Chem. Phys., 7, 1585–1598, doi:10.5194/acp-7-1585-2007, 2007.
Drewnick, F., Hings, S. S., DeCarlo, P., Jayne, J. T., Gonin, M., Fuhrer, K., Weimer, S., Jimenez, J. L., Demerjian, K. L., Borrmann, S., and Worsnop, D. R.: A new time-of-flight aerosol mass spectrometer (TOF-AMS) – instrument description and first field deployment, Aerosol Sci. Tech., 39, 637–658, doi:10.1080/02786820500182040, 2005.
Fehsenfeld, F. C., Ancellet, G., Bates, T. S., Goldstein, A. H., Hardesty, R. M., Honrath, R., Law, K. S., Lewis, A. C., Leaitch, R., McKeen, S., Meagher, J., Parrish, D. D., Pszenny, A. A. P., Russell, P. B., Schlager, H., Seinfeld, J., Talbot, R., and Zbinden, R.: International Consortium for Atmospheric Research on Transport and Transformation (ICARTT): North America to Europe – overview of the 2004 summer field study, J. Geophys. Res., 111, D23S01, doi:10.1029/2006JD007829, 2006.
Finessi, E., Decesari, S., Paglione, M., Giulianelli, L., Carbone, C., Gilardoni, S., Fuzzi, S., Saarikoski, S., Raatikainen, T., Hillamo, R., Allan, J., Mentel, Th. F., Tiitta, P., Laaksonen, A., Petäjä, T., Kulmala, M., Worsnop, D. R., and Facchini, M. C.: Determination of the biogenic secondary organic aerosol fraction in the boreal forest by NMR spectroscopy, Atmos. Chem. Phys., 12, 941–959, doi:10.5194/acp-12-941-2012, 2012.
Gard, E., Mayer, J. E., Morrical, B. D., Dienes, T., Fergenson, D. P., and Prather, K. A.: Real-time analysis of individual atmospheric aerosol particles: design and performance of a portable ATOFMS, Anal. Chem., 69, 4083–4091, 1997.
Gilge, S., Plass-Duelmer, C., Fricke, W., Kaiser, A., Ries, L., Buchmann, B., and Steinbacher, M.: Ozone, carbon monoxide and nitrogen oxides time series at four alpine GAW mountain stations in central Europe, Atmos. Chem. Phys., 10, 12295–12316, doi:10.5194/acp-10-12295-2010, 2010.
Graber, E. R. and Rudich, Y.: Atmospheric HULIS: How humic-like are they? A comprehensive and critical review, Atmos. Chem. Phys., 6, 729–753, doi:10.5194/acp-6-729-2006, 2006.
Harrison, R. M., Dall'Osto, M., Beddows, D. C. S., Thorpe, A. J., Bloss, W. J., Allan, J. D., Coe, H., Dorsey, J. R., Gallagher, M., Martin, C., Whitehead, J., Williams, P. I., Jones, R. L., Langridge, J. M., Benton, A. K., Ball, S. M., Langford, B., Hewitt, C. N., Davison, B., Martin, D., Petersson, K. F., Henshaw, S. J., White, I. R., Shallcross, D. E., Barlow, J. F., Dunbar, T., Davies, F., Nemitz, E., Phillips, G. J., Helfter, C., Di Marco, C. F., and Smith, S.: Atmospheric chemistry and physics in the atmosphere of a developed megacity (London): an overview

ACPD
14, 9275–9343, 2014

of the REPARTEE experiment and its conclusions, Atmos. Chem. Phys., 12, 3065–3114, doi:10.5194/acp-12-3065-2012, 2012.

Hayes, P. L., Ortega, A. M., Cubison, M. J., Froyd, K. D., Zhao, Y., Cliff, S. S., Hu, W. W., Toohey, D. W., Flynn, J. H., Lefer, B. L., Grossberg, N., Alvarez, S., Rappenglück, B., Taylor, J. W., Allan, J. D., Holloway, J. S., Gilman, J. B., Kuster, W. C., de Gouw, J. A., Massoli, P., Zhang, X., Liu, J., Weber, R. J., Corrigan, A. L., Russell, L. M., Isaacman, G., Worton, D. R., Kreisberg, N. M., Goldstein, A. H., Thalman, R., Waxman, E. M., Volkamer, R., Lin, Y. H., Surratt, J. D., Kleindienst, T. E., Offenberg, J. H., Dusanter, S., Griffith, S., Stevens, P. S., Brioude, J., Angevine, W. M., and Jimenez, J. L.: Organic aerosol composition and sources in Pasadena, California, during the 2010 CalNex campaign, J. Geophys. Res., 118, 9233–9257, doi:10.1002/jgrd.50530, 2013.

Healy, R. M., Sciare, J., Poulain, L., Crippa, M., Wiedensohler, A., Prévôt, A. S. H., Baltensperger, U., Sarda-Estève, R., McGuire, M. L., Jeong, C.-H., McGillicuddy, E., O'Connor, I. P., Sodeau, J. R., Evans, G. J., and Wenger, J. C.: Quantitative determination of carbonaceous particle mixing state in Paris using single-particle mass spectrometer and aerosol mass spectrometer measurements, Atmos. Chem. Phys., 13, 9479–9496, doi:10.5194/acp-13-9479-2013, 2013.

Henne, S., Furger, M., Nyeki, S., Steinbacher, M., Neininger, B., de Wekker, S. F. J., Dommen, J., Spichtinger, N., Stohl, A., and Prévôt, A. S. H.: Quantification of topographic venting of boundary layer air to the free troposphere, Atmos. Chem. Phys., 4, 497–509, doi:10.5194/acp-4-497-2004, 2004.

Jaumot, J., Gargallo, R., de Juan, A., and Tauler, R.: A graphical userfriendly interface for MCR_ALS: a new tool for multivariate curve resolution in MATLAB, Chemometr. Intell. Lab., 76, 101–110, doi:10.1016/j.chemolab.2004.12.007, 2005.

Jayne, J. T., Leard, D. C., Zhang, X. F., Davidovits, P., Smith, K. A., Kolb, C. E., and Worsnop, D. R.: Development of an aerosol mass spectrometer for size and composition analysis of submicron particles, Aerosol Sci. Tech., 33, 49–70, 2000.

Jimenez, J. L., Jayne, J. T., Shi, Q., Kolb, C. E., Worsnop, D. R., Yourshaw, I., Seinfeld, J. H., Flagan, R. C., Zhang, X. F., Smith, K. A., Morris, J. W., and Davidovits, P.: Ambient aerosol sampling using the Aerodyne Aerosol Mass Spectrometer, J. Geophys. Res.-Atmos., 108, 8425, doi:10.1029/2001JD001213, 2003.

Jimenez, J. L., Canagaratna, M. R., Donahue, N. M., Prevot, A. S. H., Zhang, Q., Kroll, J. H., DeCarlo, P. F., Allan, J. D., Coe, H., Ng, N. L., Aiken, A. C., Docherty, K. S., Ulbrich, I. M.,

ACPD
14, 9275–9343, 2014

Grieshop, A. P., Robinson, A. L., Duplissy, J., Smith, J. D., Wilson, K. R., Lanz, V. A., Hueglin, C., Sun, Y. L., Tian, J., Laaksonen, A., Raatikainen, T., Rautiainen, J., Vaattovaara, P., Ehn, M., Kulmala, M., Tomlinson, J. M., Collins, D. R., Cubison, M. J., Dunlea, E. J., Huffman, J. A., Onasch, T. B., Alfarra, M. R., Williams, P. I., Bower, K., Kondo, Y., Schneider, J., Drewnick, F., Borrmann, S., Weimer, S., Demerjian, K., Salcedo, D., Cottrell, L., Griffin, R., Takami, A., Miyoshi, T., Hatakeyama, S., Shimono, A., Sun, J. Y., Zhang, Y. M., Dzepina, K., Kimmel, J. R., Sueper, D., Jayne, J. T., Herndon, S. C., Trimborn, A. M., Williams, L. R., Wood, E. C., Middlebrook, A. M., Kolb, C. E., Baltensperger, U., and Worsnop, D. R.: Evolution of organic aerosols in the atmosphere, Science, 326, 1525–1529, 2009.

Kleinman, L., Lee, Y.-N., Springston, S. R., Nunnermacker, L., Zhou, X., Brown, R., Hallock, K., Klotz, P., Leahy, D., Lee, J. H., Newman, L.: Ozone formation at a rural site in the southeastern United States, J. Geophys. Res., 99, 3469–3482, 1994.

Kulmala, M., Asmi, A., Lappalainen, H. K., Baltensperger, U., Brenguier, J.-L., Facchini, M. C., Hansson, H.-C., Hov, Ø., O'Dowd, C. D., Pöschl, U., Wiedensohler, A., Boers, R., Boucher, O., de Leeuw, G., Denier van der Gon, H. A. C., Feichter, J., Krejci, R., Laj, P., Lihavainen, H., Lohmann, U., McFiggans, G., Mentel, T., Pilinis, C., Riipinen, I., Schulz, M., Stohl, A., Swietlicki, E., Vignati, E., Alves, C., Amann, M., Ammann, M., Arabas, S., Artaxo, P., Baars, H., Beddows, D. C. S., Bergström, R., Beukes, J. P., Bilde, M., Burkhart, J. F., Canonaco, F., Clegg, S. L., Coe, H., Crumeyrolle, S., D'Anna, B., Decesari, S., Gilardoni, S., Fischer, M., Fjaeraa, A. M., Fountoukis, C., George, C., Gomes, L., Halloran, P., Hamburger, T., Harrison, R. M., Herrmann, H., Hoffmann, T., Hoose, C., Hu, M., Hyvärinen, A., Hõrrak, U., Iinuma, Y., Iversen, T., Josipovic, M., Kanakidou, M., Kiendler-Scharr, A., Kirkevåg, A., Kiss, G., Klimont, Z., Kolmonen, P., Komppula, M., Kristjánsson, J.-E., Laakso, L., Laaksonen, A., Labonnote, L., Lanz, V. A., Lehtinen, K. E. J., Rizzo, L. V., Makkonen, R., Manninen, H. E., McMeeking, G., Merikanto, J., Minikin, A., Mirme, S., Morgan, W. T., Nemitz, E., O'Donnell, D., Panwar, T. S., Pawlowska, H., Petzold, A., Pienaar, J. J., Pio, C., Plass-Duelmer, C., Prévôt, A. S. H., Pryor, S., Reddington, C. L., Roberts, G., Rosenfeld, D., Schwarz, J., Seland, Ø., Sellegri, K., Shen, X. J., Shiraiwa, M., Siebert, H., Sierau, B., Simpson, D., Sun, J. Y., Topping, D., Tunved, P., Vaattovaara, P., Vakkari, V., Veefkind, J. P., Visschedijk, A., Vuollekoski, H., Vuolo, R., Wehner, B., Wildt, J., Woodward, S., Worsnop, D. R., van Zadelhoff, G.-J., Zardini, A. A., Zhang, K., van Zyl, P. G., Kerminen, V.-M., S Carslaw, K., and Pandis, S. N.: General overview: European Integrated project on Aerosol Cloud Climate and Air Quality interactions (EUCAARI) – integrating aerosol re-

ACPD
14, 9275–9343, 2014

search from nano to global scales, Atmos. Chem. Phys., 11, 13061–13143, doi:10.5194/acp-11-13061-2011, 2011.
Lanz, V. A., Alfarra, M. R., Baltensperger, U., Buchmann, B., Hueglin, C., and Prévôt, A. S. H.: Source apportionment of submicron organic aerosols at an urban site by factor analytical modelling of aerosol mass spectra, Atmos. Chem. Phys., 7, 1503–1522, doi:10.5194/acp-7-1503-2007, 2007.
Larssen, S., Sluyter, R., and Helmis, C.: Criteria for EUROAIRNET, the EEA Air Quality Monitoring and Information Network. Technical Report No.12, European Environmental Agency, Copenhagen, 1999.
Laskin, A., Laskin, J., and Nizkorodov, S. A.: Mass spectrometric approaches for chemical characterisation of atmospheric aerosols: critical review of the most recent advances, Environ. Chem., 9, 163–189, 2012.
Lin, C.-J.: Projected gradient methods for non-negative matrix factorization, Neural Comput., 19, 2756–2779, doi:10.1162/neco.2007.19.10.2756, 2007.
Matta, E., Facchini, M. C., Decesari, S., Mircea, M., Cavalli, F., Fuzzi, S., Putaud, J.-P., and Dell'Acqua, A.: Mass closure on the chemical species in size-segregated atmospheric aerosol collected in an urban area of the Po Valley, Italy, Atmos. Chem. Phys., 3, 623–637, doi:10.5194/acp-3-623-2003, 2003.
McLafferty, F. W.: Interpretation of Mass Spectra, 3rd edn., 303 pp., University Science Books, Sausalito (CA), USA, 1993.
Middlebrook, A. M., Bahreini, R., Jimenez, J. L., and Canagaratna, M. R.: Evaluation of composition-dependent collection efficiencies for the aerodyne aerosol mass spectrometer using field data, Aerosol Sci. Tech., 46, 258–271, 2012.
Mohr, C., DeCarlo, P. F., Heringa, M. F., Chirico, R., Slowik, J. G., Richter, R., Reche, C., Alastuey, A., Querol, X., Seco, R., Peñuelas, J., Jiménez, J. L., Crippa, M., Zimmermann, R., Baltensperger, U., and Prévôt, A. S. H.: Identification and quantification of organic aerosol from cooking and other sources in Barcelona using aerosol mass spectrometer data, Atmos. Chem. Phys., 12, 1649–1665, doi:10.5194/acp-12-1649-2012, 2012.
Onasch, T. B., Trimborn, A., Fortner, E. C., Jayne, J. T., Kok, G. L., Williams, L. R., Davidovits, P., and Worsnop, D. R.: Soot particle aerosol mass spectrometer: development, validation, and initial application, Aerosol Sci. Tech., 46, 804–817, 2012.

ACPD
14, 9275–9343, 2014

Paatero, P. and Tapper, U.: Positive Matrix Factorization: a nonnegative factor model with optimal utilization of error estimates of data values, Environmetrics, 5, 111–126, doi:10.1002/env.3170050203, 1994.

Paglione, M., Saarikoski, S., Carbone, S., Hillamo, R., Facchini, M. C., Finessi, E., Giulianelli, L., Carbone, C., Fuzzi, S., Moretti, F., Tagliavini, E., Swietlicki, E., Eriksson Stenström, K., Prévôt, A. S. H., Massoli, P., Canaragatna, M., Worsnop, D., and Decesari, S.: Primary and secondary biomass burning aerosols determined by proton nuclear magnetic resonance (H-NMR) spectroscopy during the 2008 EUCAARI campaign in the Po Valley (Italy), Atmos. Chem. Phys. Discuss., 13, 33343–33401, doi:10.5194/acpd-13-33343-2013, 2013.

Plass-Dülmer, C., Elste, T., Paasonen, P., and Petäjä, T.: Sulfuric Acid Measurements by CIMS – Uncertainties and Consistency between Various Data Sets, Poster presentation at EGU General Assembly 2011, Vienna, available at: http://presentations.copernicus.org/EGU2011-11691_presentation.ppt (last access: 1 April 2014), 2011.

Rinaldi, M., Emblico, L., Decesari, S., Fuzzi, S., Facchini, M. C., and Librando, V.: Chemical characterization and source apportionment of size-segregated aerosol collected at an urban site in Sicily, Water Air Soil Poll., 185, 311–321, 2007.

Rohrer, F. and Berresheim, H.: Strong correlation between levels of tropospheric hydroxyl radicals and solar ultraviolet radiation, Nature, 442, 7099, 184–187, doi:10.1038/nature04924, 2006.

Saarikoski, S., Carbone, S., Decesari, S., Giulianelli, L., Angelini, F., Canagaratna, M., Ng, N. L., Trimborn, A., Facchini, M. C., Fuzzi, S., Hillamo, R., and Worsnop, D.: Chemical characterization of springtime submicrometer aerosol in Po Valley, Italy, Atmos. Chem. Phys., 12, 8401–8421, doi:10.5194/acp-12-8401-2012, 2012.

Song, X. H., Hopke, P. K., Fergenson, D. P., and Prather, K. A.: Classification of single particles analyzed by ATOFMS using an artificial neural network, ART-2A, Anal. Chem., 71, 860–865, 1999.

Tauler, R.: Multivariate curve resolution applied to second order data, Chemometr. Intell. Lab., 30, 133–146, doi:10.1016/0169-7439(95)00047-X, 1995.

Ulbrich, I. M., Canagaratna, M. R., Zhang, Q., Worsnop, D. R., and Jimenez, J. L.: Interpretation of organic components from Positive Matrix Factorization of aerosol mass spectrometric data, Atmos. Chem. Phys., 9, 2891–2918, doi:10.5194/acp-9-2891-2009, 2009.

ACPD
14, 9275–9343, 2014

Virkkula, A., Ahlquist, N. C., Covert, D. S., Arnott, W. P., Sheridan, P. J., Quinn, P. K., and Coffman, D. J.: Modification, calibration and a field test of an instrument for measuring light absorption by particles, Aerosol Sci. Tech., 39, 68–83, 2005.

Williams, B. J., Goldstein, A. H., Kreisberg, N. M., and Hering, S. V.: An in-situ instrument for speciated organic composition of atmospheric aerosols: thermal desorption Aerosol GC/MS-FID (TAG), Aerosol Sci. Technol., 40, 627–638, 2006.

Williams, B. J., Goldstein, A. H., Kreisberg, N. M., Hering, S. V., Worsnop, D. R., Ulbrich, I. M., Docherty, K. S., and Jimenez, J. L.: Major components of atmospheric organic aerosol in southern California as determined by hourly measurements of source marker compounds, Atmos. Chem. Phys., 10, 11577–11603, doi:10.5194/acp-10-11577-2010, 2010.

Williams, B. J., Jayne, J. T., Lambe, A. T., Hohaus, T., Kimmel, J. R., Sueper, D., Brooks, W., Williams, L. R., Trimborn, A. M., Martinez, R. E., Hayes, P. L., Jimenez, J. L., Kreisberg, N. M., Hering, S. V., Worton, D. R., Goldstein, A. H., and Worsnop, D. R.: The first combined thermal desorption aerosol gas chromatograph–aerosol mass spectrometer (TAG-AMS), Aerosol Sci. Technol, 48, 358–370, 2014.

Wood, E. C., Canagaratna, M. R., Herndon, S. C., Onasch, T. B., Kolb, C. E., Worsnop, D. R., Kroll, J. H., Knighton, W. B., Seila, R., Zavala, M., Molina, L. T., DeCarlo, P. F., Jimenez, J. L., Weinheimer, A. J., Knapp, D. J., Jobson, B. T., Stutz, J., Kuster, W. C., and Williams, E. J.: Investigation of the correlation between odd oxygen and secondary organic aerosol in Mexico City and Houston, Atmos. Chem. Phys., 10, 8947–8968, doi:10.5194/acp-10-8947-2010, 2010.

Zanatta, M., Cavalli, F., Gysel, M., Weingartner, E., Baltensperger, U., and Laj, P.: Black carbon (BC) absorbing properties over Europe, in preparation, 2014.

Zhang, Y., Williams, B. J., Goldstein, A. H., Ulbrich, I. M., Docherty, K., and Jimenez, J. L.: A technique for rapid gas chromatography analysis applied to ambient organic aerosol measurements from the thermal desorption aerosol gas chromatograph (TAG), Aerosol Sci. Technol., submitted, 2014.

ACPD
14, 9275–9343, 2014

Table 1. ATOFMS clusters.

cluster	N particle	%
NIT-Reg	24 409	48
NIT-Local	10 979	22
EC-Reg	5902	12
SUL-Reg	1910	4
CN-Amines	1368	3
NIT-Local/Reg	1419	3
OC-NIT-SUL	1208	2
NaCl	3114	6
spikes	548	1
TOT	50 857	100

ACPD
14, 9275–9343, 2014

Table 2. Correlation (r^2) between AMS factors and chemical components, and ATOFMS clusters (3 h averages).

	AMS LVOOA MO	AMS LVOOA LO	AMS SV-OOA	AMS HOA	AMS COA	AMS Cl^-	AMS NO_3^-	AMS SO_4^{2-}	AMS Org	AMS NH_4^+	PSAP BC
ATOFMS NIT-REG	0.48			0.4			0.3		0.35	0.35	0.4
ATOFMS NIT-LOCAL				0.45					0.37		0.55
ATOFMS EC	0.65							0.35			0.45
ATOFMS EC-SUL	0.45							0.4			
ATOFMS CN-AMINE		0.3		0.4					0.41		
ATOFMS EC-K-NIT									0.4		
ATOFMS OC-NIT-SUL			0.7		0.55				0.4		

ACPD
14, 9275–9343, 2014

Table 3. Correlation coefficient (as r^2, negative in bold cells) of NMR factors for WSOC with submicron inorganic aerosol components and with trace gases. Only coefficients greater than 0.2 (as absolute value) are shown.

	nssCl	nss SO_4^{2-}	NO_3^-	NH_4^+	nssK	sea salt	BC	SO_2	NO	NO_2
NMR F1	0.25		0.34	0.20			0.36			
NMR F2										
NMR F3	0.28									
NMR F4		0.51						0.28		**0.24**
NMR F1 + F2 ("non HULIS")							0.20			0.21
NMR F3 + F4 ("HULIS")							0.28			

ACPD
14, 9275–9343, 2014

Table 4. Correlation between AMS and NMR factors. Only correlations (r^2) higher than 0.2 are listed, if not left blank. All correlations shown are positive.

	(LV)OOA MO	(LV)OOA LO	SV-OOA	HOA	COA	(LV)OOA LO + MO	SV-OOA + COA
NMR F1			0.45		0.23		0.41
NMR F2							
NMR F3		0.49					
NMR F4	0.61					0.53	
NMR F1 + F2 (non-HULIS)			0.40	0.22	0.39		0.48
NMR F3 + F4 (HULIS)			0.25	0.31	0.26	0.51	

ACPD
14, 9275–9343, 2014

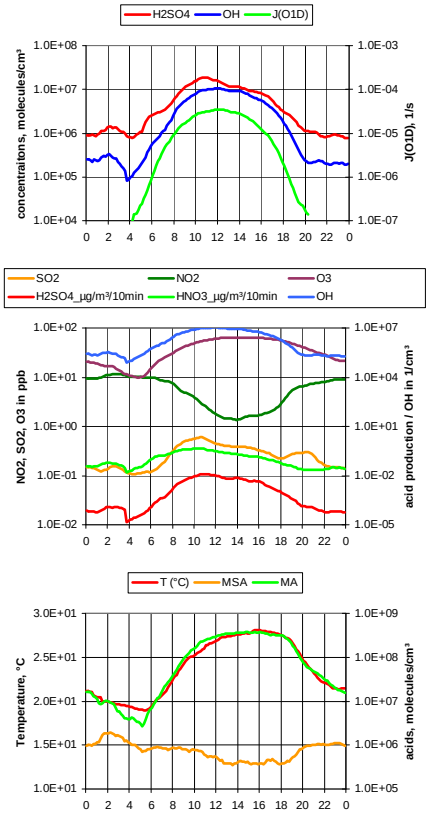

Fig. 1. Mean daily cycles of gas-phase compounds. Upper panel: OH and H_2SO_4 concentrations and $J(O^1D)$; middle panel: mixing ratios of SO_2, NO_2, and O_3 (left), OH concentration (molecules cm^{-3}) and the formation rates of H_2SO_4 and HNO_3 ($\mu g\,m^{-3}/10\,min$) (right axis); lower panel: temperature and acid concentrations (MSA: methanesulphonic acid, MA: malonic acid).

ACPD
14, 9275–9343, 2014

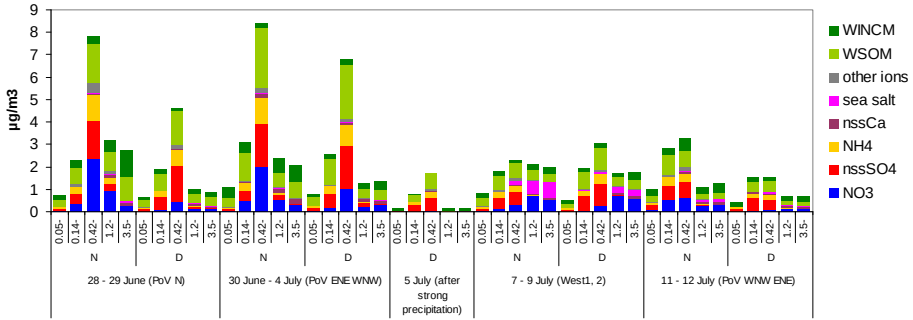

Fig. 2. Size-segregated aerosol compositions from 5-stage Berner impactors. Averages for five periods of the campaign and for night (N) and day (D) samples are shown. For each period, prevalent back-trajectory types are reported. The impactor size intervals (as ambient aerodynamic diameters) corresponding to the stages are: 0.05–0.14, 0.14–0.42, 0.42–1.2, 1.2–3.5, 3.5–10 µm. WSOM (water-soluble organic matter) = WSOC · 1.9; WINCM (water-insoluble carbonaceous matter) = (TC-WSOC) · 1.2.

ACPD
14, 9275–9343, 2014

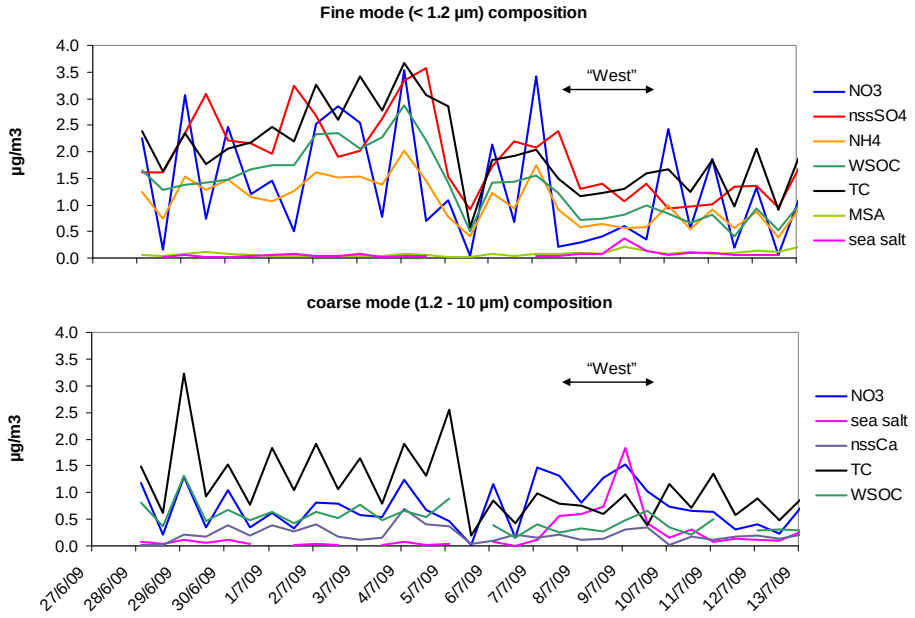

Fig. 3. Time trends of main fine and coarse aerosol chemical components. The x-axis reports the mean time in each sampling interval. Days characterized by westerly air masses are indicated in the figure.

ACPD
14, 9275–9343, 2014

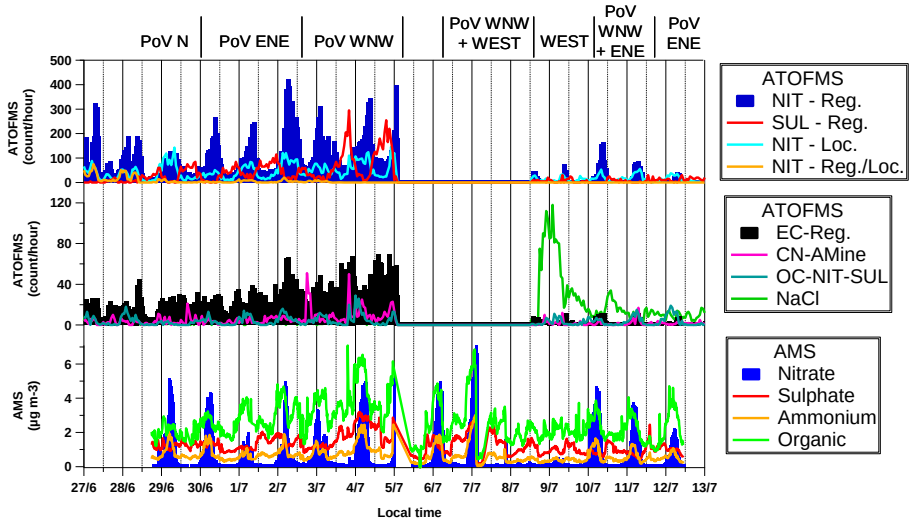

Fig. 4. AMS general trends, and ATOFMS main clusters.

ACPD
14, 9275–9343, 2014

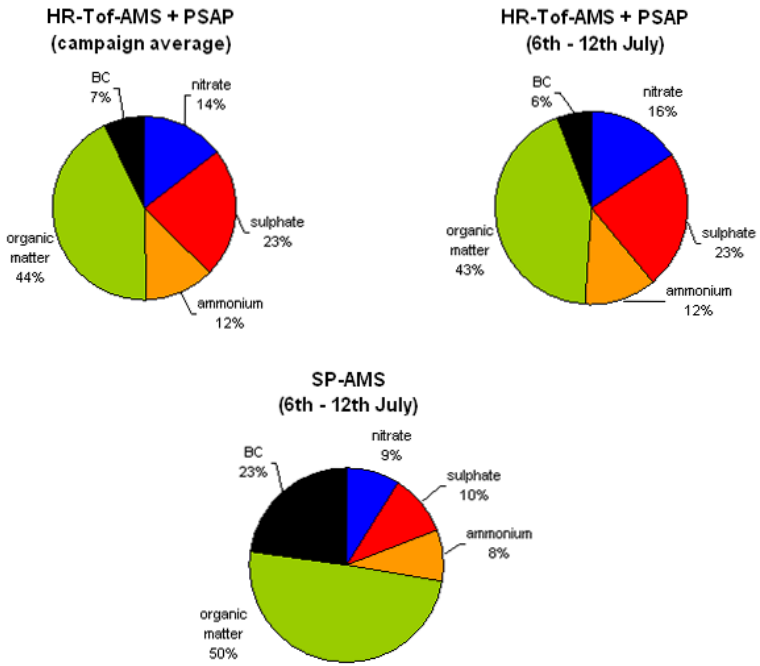

Fig. 5. Average PM_1 chemical composition from HR-TOF-AMS and SP-AMS.

ACPD
14, 9275–9343, 2014

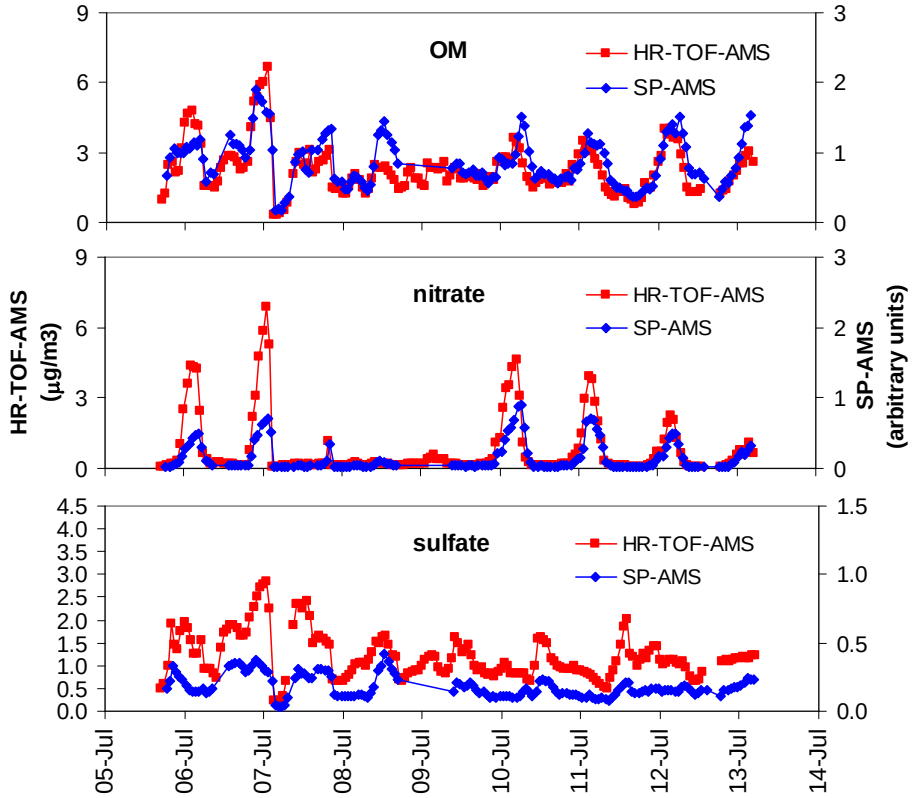

Fig. 6. Temporal trends of organic matter, nitrate and sulphate obtained by SP-AMS and HR-TOF-AMS. The vertical scale for SP-AMS is three times amplified with respect to the scale for the HR-TOF.

ACPD
14, 9275–9343, 2014

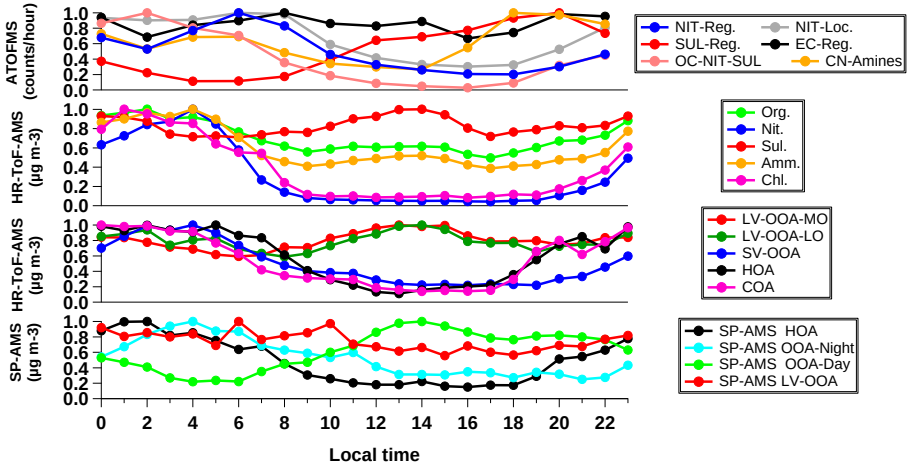

Fig. 7. Diurnal trends of the main aerosol components from (top to bottom): ATOFMS, HR-TOF-AMS (OM, ionic components), HR-TOF-AMS (PMF factors), and SP-AMS PMF factors.

ACPD
14, 9275–9343, 2014

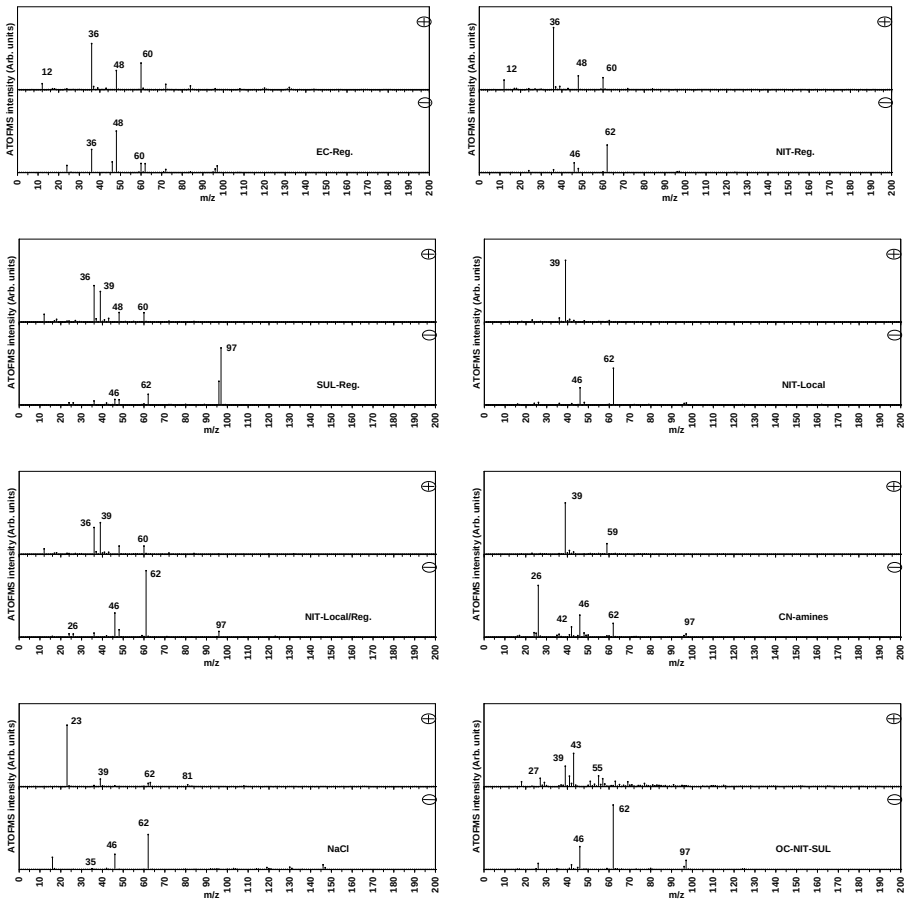

Fig. 8. Mass spectra of the ATOFMS clusters.

ACPD
14, 9275–9343, 2014

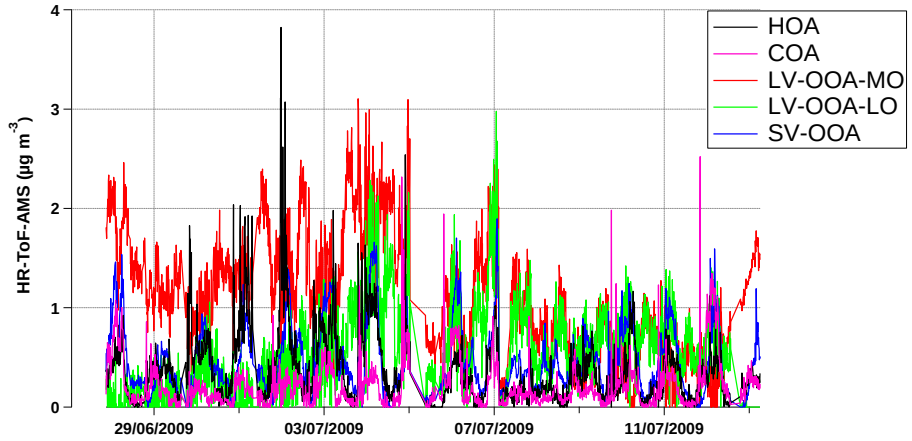

Fig. 9. Temporal trend of the five HR-TOF-AMS organic factors.

ACPD
14, 9275–9343, 2014

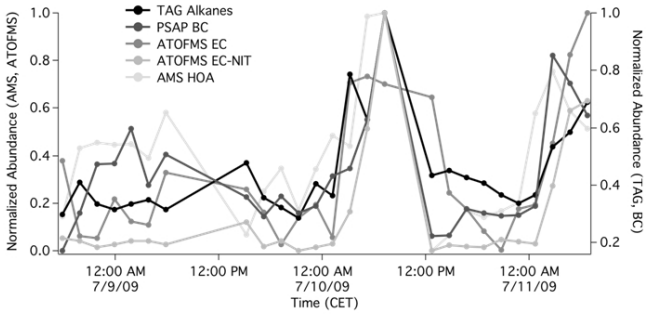

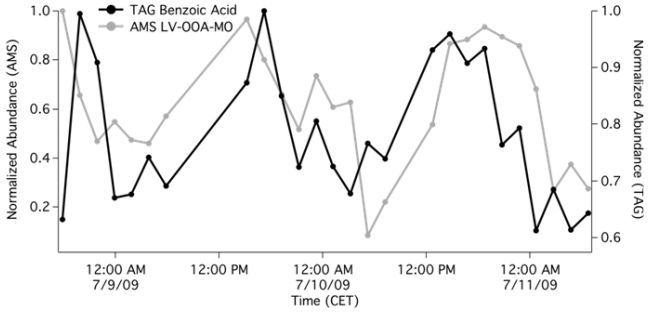

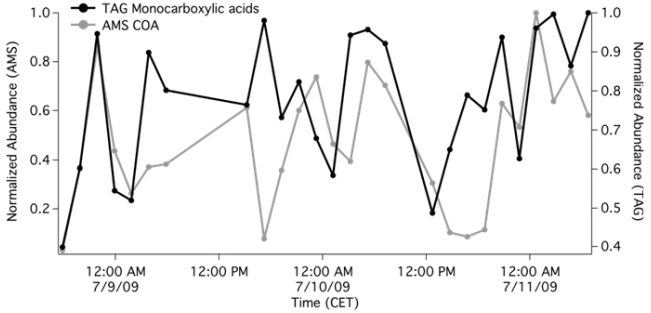

ACPD
14, 9275–9343, 2014

Aerosol chemical composition and mixing state in the Po Valley

S. Decesari et al.

Fig. 10. Time trends of major chemical classes measured by HR-ToFMS-TAG, shown together with the correlated external tracers from other techniques: **(a)** TAG alkanes (two combined factors) vs. PSAP BC, AMS HOA, ATOFMS EC-NIT (NIT-REG), and ATOFMS EC, **(b)** TAG benzoic acid vs. AMS LV-OOA-MO, **(c)** TAG monocarboxylic acids (two combined factors) vs. AMS COA.

ACPD
14, 9275–9343, 2014

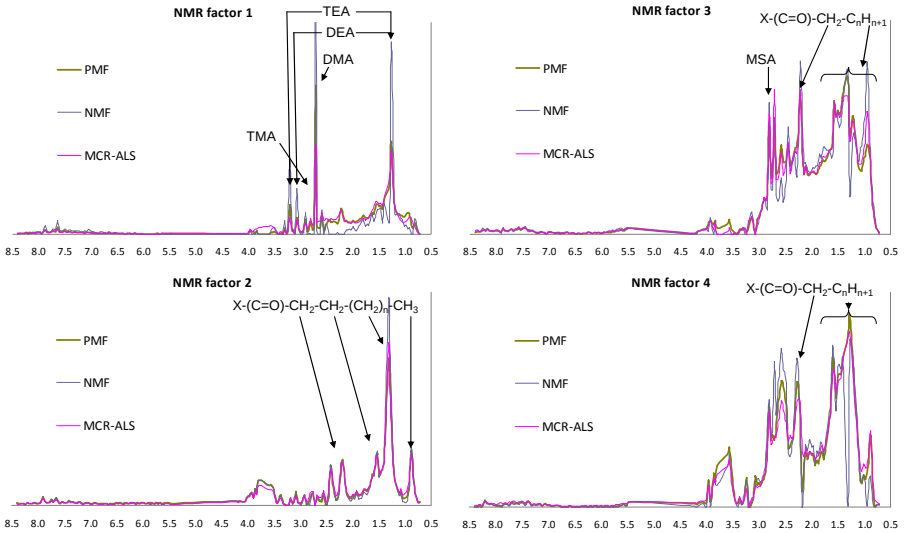

Fig. 11. NMR spectral profiles of the four factors. The *x*-axis reports the NMR chemical shift (ppm).

ACPD
14, 9275–9343, 2014

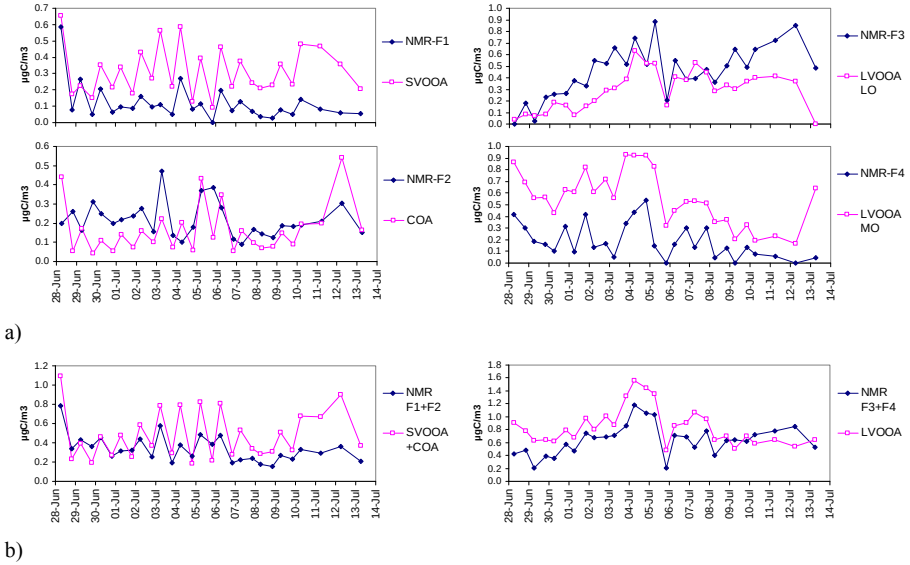

Fig. 12. (a, b) Comparison of time trends of NMR factors (PMF solution) and time-integrated AMS factor concentrations. HOA is left out since it is not expected to contribute to WSOC. The y-axis reports concentrations in $\mu g C m^{-3}$.

ACPD
14, 9275–9343, 2014

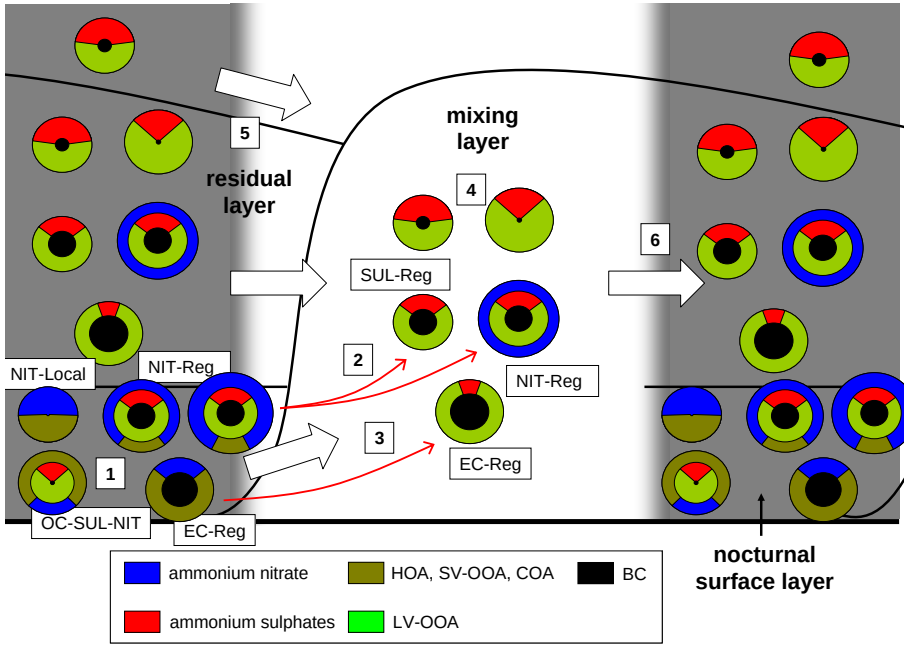

Fig. 13. Schematic representation of the evolution of accumulation mode aerosol chemical composition and mixing state during the field campaign. Grey and white areas represent night and day hours. The vertical axis is the elevation above ground level. The thickness of the nocturnal surface layer is approximately 100–500 m. The height of the daytime mixing layer is 1500–2000 m above the ground.

ACPD
14, 9275–9343, 2014

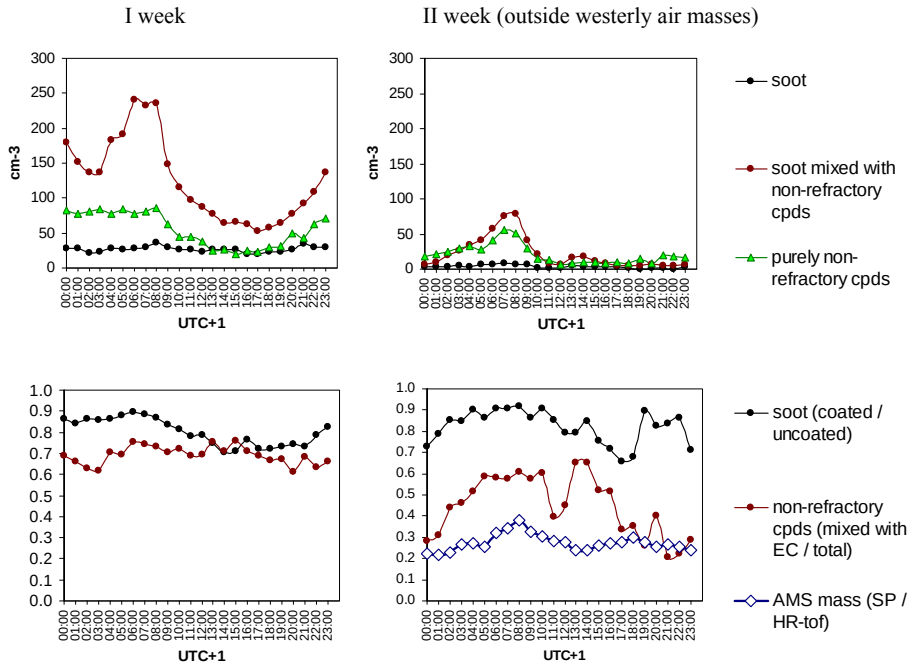

Fig. 14. Upper panels: summary of the diurnal cycles of main ATOFMS particle populations: soot (EC), coated soot (i.e., soot mixed with non-refractory components) (EC-NIT + EC-SUL + K-EC-NIT), purely non-refractory particles (i.e., unmixed with soot) (K-NIT + KCN + OC-SUL-NIT). Lower panels: concentration ratios between the main ATOFMS particle populations. The two panels on the left refer to the first week of campaign, while the ones on the left cover the three last days of the experiment (when ATOFMS and SP-AMS were operated in parallel). The mass ratio between total non-refractory components mass from the SP-AMS and from the HR-Tof-AMS is shown in the bottom-right panel.

ACPD
14, 9275–9343, 2014

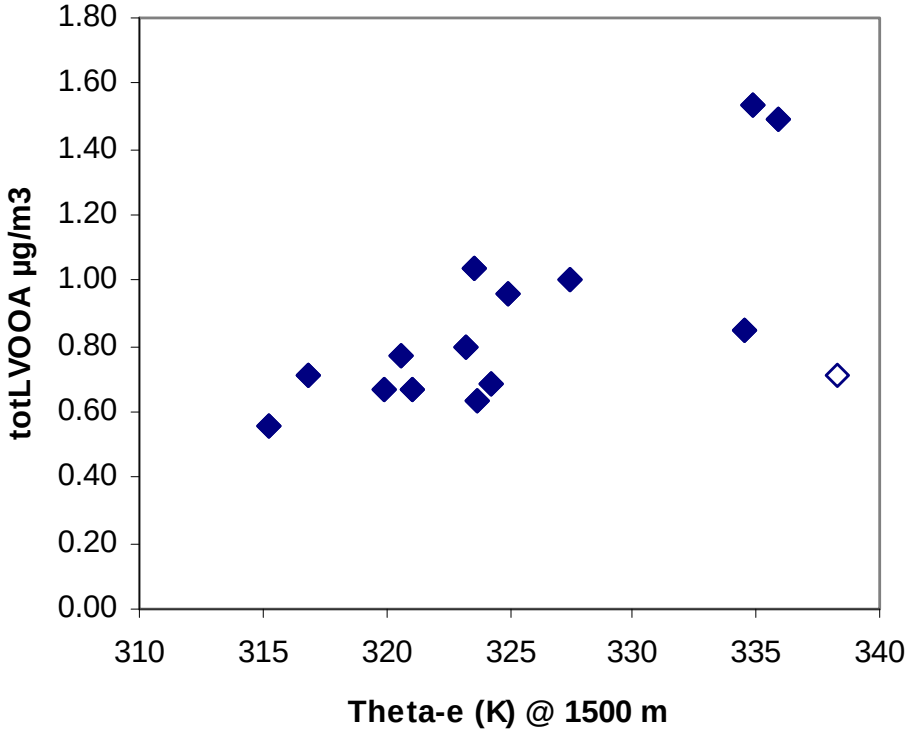

Fig. 15. Scatter plot between equivalent potential temperature and total LV-OOA. The white symbol corresponds to the 5 July sample.

ACPD
14, 9275–9343, 2014